UNIVERSITY OF OKLAHOMA

GRADUATE COLLEGE

CHARACTERIZATION OF THE SYCAMORE FORMATION, VELMA FIELD, ARDMORE BASIN OKLAHOMA

A THESIS

SUBMITTED TO THE GRADUATE FACULTY

in partial fulfillment of the requirements for the

Degree of

MASTER OF SCIENCE

By

SOFIA ALLBEE CAYLOR
Norman, Oklahoma
2019

CHARACTERIZATION OF THE SYCAMORE FORMATION, VELMA FIELD, ARDMORE BASIN OKLAHOMA

A THESIS APPROVED FOR THE

CONOCOPHILLIPS SCHOOL OF GEOLOGY AND GEOPHYSICS

BY

Dr. Roger M. Slatt, Chair

Dr. Richard Douglas Elmore

Dr. David DeFelice

© Copyright by SOFIA ALLBEE CAYLOR 2019
All Rights Reserved.

For my grandmother Magdalena, who instilled in me the importance of education from the beginning. I would not be here today without you and your loving care that has pushed me onto a bright future. Mamita, this is for you.

ACKNOWLEDGEMENTS

First, I would like to thank Dr. Roger Slatt for the opportunity to pursue a master's degree under his guidance and complete a thesis project as a graduate student member of the IRC. I have truly learned so much from your tenacity as a geologist and your kindness as an advisor. Thank you for all that you have done for all of us students, for believing in us, and shaping us up. It has been both a pleasure and an honor. Thank you.

I would like to thank my committee members. Dr. Doug Elmore for his guidance with my thesis and commitment to his students. I also thank Dr. David DeFelice for his commitment to my thesis as well and for his unceasing belief in investing in the oil and gas industry's future, in the students.

I would like to thank all company participants of the IRC, especially 89 Energy for investing in the STACK -MERGE – SCOOP consortium and for donating data to my project. I am forever grateful.

I would like to thank the Oklahoma Petroleum Information Center for all their time and for the opportunity to observe and test my core in such detail. Special thanks go to Vyetta Jordan and Jeffery Dillon for all their coordination and flexibility during the core viewing process. Also special thanks to Dr. Abbas Seyedolali of the Oklahoma Geological Survey for his assistance with understanding bioturbation and sedimentary features within this core. His assistance was monumental for this project.

I would also like to thank Patricio Desjardins for taking time to teach us about core viewing and observation processes and for pointing out some key ideas about the Sycamore Formation, that were critical to this project.

Special thanks to all the professors who have supported me along the way, especially Dr. John Pigott, Dr. Kurt Marfurt, and Dr. Andy Madden.

I would also like to thank Rebecca Fay for her guidance with the graduate student processes, and all the staff within the CPSGG office. You make the department run, and we are all very grateful for all that you do as a team.

I would like to also thank my fellow IRC students, Emilio Torres, Jing Zhang, Benmadi Milad, David Duarte, Andreina Liborius, Antonio Cervantes, Austin McGlannan, Carlos Molinares, Richard Brito, Delcio Teixeira, Karelia La Marca, Lindy Dingmore, Dalila Jesus, Ryan Rosol, Muizz Matemilola, Francis Oyebanji, and Eva Perez. It has been a pleasure working with you all and your input has been important to the development of this project. This was possible with your input and I am so grateful to have walked this journey with you all. Thank you!

I would also like to thank my peers, Desiree Hullaster, Carl Symcox, Brittney Tamborello, Gabriel Machado, and all who have contributed to this project and time during graduate school.

I would also like to thank my peers and colleagues at BP Alaska. Special thanks to Keith Robertson and Priya Maraj. Your encouragement and guidance during summer 2018 sparked and fueled the furtherment of this project.

I would like to thank the West Texas Geological Society for all their dedication and support over the course of my geoscience education. Your passion for rocks was contagious and has always pushed me to be a better geoscientist. Special thanks go to Paula Sanchez, Curtis Helms, Dexter Harmon, Jeff Bryden, David Thomas III, Stonnie Polluck, Ron Bianco, and everyone who mentored and taught me along the way. You all have played a critical role in being exemplary geoscientists and professionals while mentoring me. Your vision has made a real difference in my life, and I am most grateful!

I would also like to thank my roommates and close friends Caitlin Schneider, Megan Lastra-Cruz, Desire Fletcher and Andrew Arsenault who were there for me during the process of this thesis.

Lastly, I would like to thank my family and above all God, for all the blessings in my life. Your never-ending faith in me, continues to push me above and beyond especially in the most difficult moments. I love you Mom, Dad, Andrew, Analicia, Emilia, Nicholas, Christina, and Liam. You all are my greatest inspiration.

TABLE OF CONTENTS

LIST OF FIGURES

LIST OF TABLES

LIST OF EQUATIONS

ABSTRACT

The Velma field is located in the northwestern extent of the Ardmore Basin in southern Oklahoma. Historically the combined Sholem- Velma- Tatums field area is one of the top producing oil and gas conventional producing fields in Oklahoma. The area has been exploited for conventional and Woodford Shale unconventional reservoir targets formerly. Attention is now being turned to potential unconventional Mississippian reservoir units, such as the Sycamore Formation. The Sycamore Formation was cored in the X-1 well by the Getty Oil Company in 1980. Unfortunately, the well was dry as a conventional reservoir target but fortunately a core was taken and observed during this study to consider the Sycamore in this area as an unconventional target.

The internal stratigraphy of the Sycamore Formation has previously been observed using traditional methods such as well log observation and petrography. This study utilizes traditional methods and employs other methods such as chemostratigraphic analysis and chemofacies analyses, that have not been employed to the Sycamore Formation. Present to this study, are 5 intervals from the lower transitional Sycamore to the Middle Sycamore shale. After evaluation these units provided information about the richness of the intermittent shales and reservoir potential of the siliciclastic and carbonate driven sections in conjunction to the shales. Essentially the four sequences of implied relative sea level rise, provide the shale intervals which possess organic material and kerogen that is mostly yet to be expelled. The Sycamore within this location is particularly shallow (5,260-5,540 ft.), and the organic material is immature within the Velma field as it did not achieve the depth of burial or subsequentially the T-max required for hydrocarbon expulsion. The formation achieves greater depth of burial in the Sholem and Tatums fields which may have provided enough heat for the onset of oil generation.

Lithofacies identified in core were used during this study and upscaled using multivariate cluster analysis into 7 chemofacies. The lithofacies are: (1) laminated mudstones, (2) bioturbated mudstones, (3) laminated bioturbated mudstones, (4) massive siltstones, (5) laminated siltstones, (6) bioturbated siltstones, (7) laminated bioturbated siltstones , (8) massive calcite cemented siltstones, (9) bioturbated calcite cemented siltstones, and (10) interbedded siltstones. Chemofacies clustered these more accurately and in a way that can be incorporated in future electrofacies generation.

1. INTRODUCTION

1.1. Scope of Thesis

Oil and gas accounts for a large amount of the global energy available and plays a key role in fueling the modern world. Oklahoma energy production is currently fourth highest in the United States next to that of the Permian basin, the northeastern US (Marcellus shale play), and south Texas. Contributing to Oklahoma's production are the Anadarko basin and the south-central Ardmore Basin. The Anadarko and northernmost Ardmore basins have been divided into three main areas of interest within industry, the STACK (Sooner Trend Anadarko Canadian & Kingfisher counties), Merge, and SCOOP (South Central Oklahoma Oil Province) plays. This study focuses on the Sycamore Formation in the southernmost extent of the SCOOP play which overlaps the northwesternmost extent of the Ardmore basin.

Prior to recent advances in drilling and well completion technologies, only conventional oil and gas reservoirs were economically viable. Since the shale boom the Woodford Shale has dominated Oklahoma oil and gas production, shifting the drilling paradigm to operate mostly on unconventional resource plays. In November 2013, Newfield Exploration Co. unveiled the STACK play. During this time, they announced their priority prospect as the Woodford Shale and additional stacked targets in the younger Mississippian Meramec (Brown, 2013). Since then the Woodford Shale has been researched extensively by companies and various organizations, particularly by the Oklahoma Geological Survey (OGS) and also by the Institute of Reservoir Characterization at the University of Oklahoma, under the primary guidance of Dr. Roger Slatt. The Woodford has since been unlocked, a term used when "a resource play is well enough

understood to be developed economically and effectively with continual drilling." (Brown, 2013).

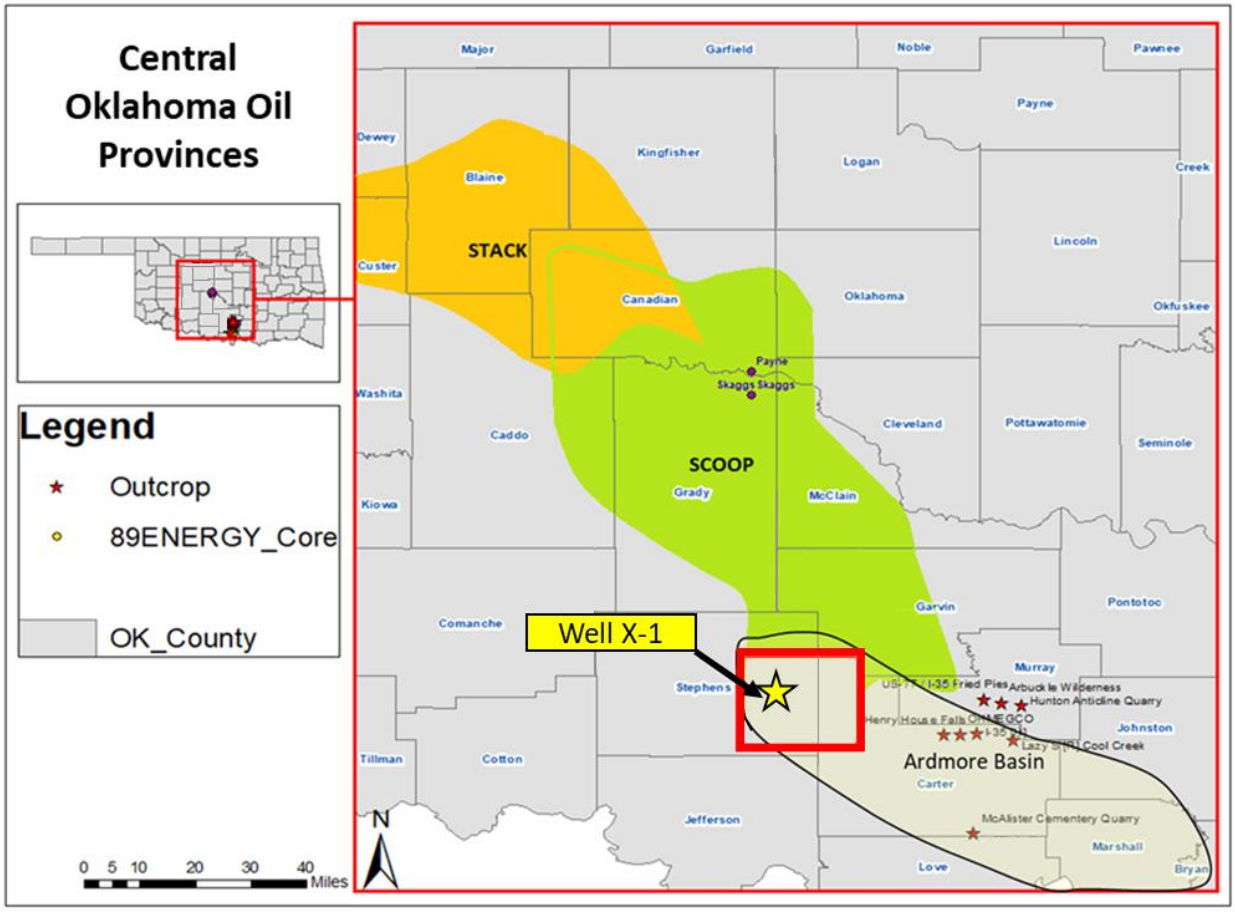

Figure 1: Map of the STACK and SCOOP in central Oklahoma with the Ardmore basin outlined. Location of the Sholem-Velma-Tatums field is within the red box and the well used in this study is labeled the X-1 and is noted by the yellow star.

The younger Sycamore Formation is of Mississippian time and is of similar age to the Meramec, if not of the same age. Unlike the Woodford shale, it is a mixed carbonate and

siliciclastic system that has not been researched as extensively and presents some unique problems geologically and as a resource play. In 1956 Pre-Pennsylvanian units were drilled in the Carter-Knox field and into the 1960's the deeper phase of drilling included targeting the Sycamore Formation. Problems such as loss of circulation and low production potential were experienced while drilling the Sycamore, deeming the unit uneconomic. "This led to by passing Sycamore pay zones for over 30 years" (Coffey, 2001), until interest in the unit picked up again in the late 1990's and early 2000's. Due to modern unconventional drilling and completion methods, the Sycamore is no longer limited to conventional well development, and potential reservoir zones that may have lacked permeability for a conventional reservoir, can be accessed via hydraulic fracturing as an unconventional resource play.

The Sycamore Formation has been described by several authors following traditional workflows of geologic and reservoir classification in various outcrop locations across the Arbuckle uplift and in subsurface in the Anadarko and Ardmore basins. This study aims to characterize the Sycamore formation in the Velma field, an area that has not been thoroughly described before. It is thought to be part of the more distal setting of the Mississippian prograding clinoforms of the high stand systems tract. The goal is to explore this distal setting idea while deepening our understanding of this rock's depositional history through careful observance of lithofacies within the Sycamore formation in the Velma field and relate this to other wells in the immediate area and to the I-35 Sycamore outcrop. By tying chemostratigraphic analysis and chemofacies classifications to the stratigraphic column of the Sycamore in the Velma field the unit may be further characterized here and provide insights that have the potential to influence facies prediction in future Sycamore studies.

1.2. Previous Research

The Sycamore Formation of central Oklahoma is considered to be a mixed carbonate and siliciclastic (Duarte, 2018; Milad, 2019; Miller, 2018) marine deposit on the gently dipping slope of the Anadarko and Ardmore basins. The Sycamore is part of the greater Mississippian deposits in this region of Oklahoma and has been correlated with other Mississippian deposits up slope such as the Meramec formation found in the STACK oil province.

Numerous authors have studied and written about the Sycamore Formation and several major sets of ideas were developed during the various periods of interest in the Sycamore. The first period began in 1903 when J. A. Taff encountered what appeared to be a limestone in the outcrop at the Sycamore Creek near Tishomingo, Oklahoma, from which he named it the Sycamore Lime (Taff, 1903). The next half decade of publications on the formation consisted of correlating the unit to other areas and classifying the age of the Sycamore using faunal age correlation and more detailed studies (Morgan, 1924). Cooper in 1926 proceeded to conduct a petrographic study of the formation in which he made note of the presence of 40% quartz grains about 10 microns in diameter, iron stains and well crystalized calcite (Cooper, 1926). Later during the period of early studies of the Sycamore formation, Weller et al., 1948 conducted a larger scale project to correlate Mississippian strata across North American geologic provinces during which time the Sycamore was noted to possibly correlate with the Osageian Mayes formation (Weller et al., 1948).

Subsequent authors worked to discern true Sycamore formation deposits from other Mississippian deposits such as the Mayes sand in in the various Oklahoma geologic provinces. In 1959, Champlin produced a study in which he placed the Sycamore as Lower Maramecian in age

while also classifying the formation to have been deposited under shallow stable conditions. Prior to Champlin's study the Sycamore had only been considered older than Meramecian.

In 1990 Schwartzapfel published his paleontological study on radiolaria. In part of the study he observed the lithostratigraphy of several units, one of which is the Sycamore Formation. During this part of the study he noted the presence of Bouma sequence features and presents the idea that the depositional mechanism responsible for the Sycamore may be turbidity currents. Through conodont zonation data he placed the Sycamore at the youngest, middle Meramecian in age.

Coffey, 2000 produced a dissertation for the Carter-Knox field. The Sycamore was a main component of the study. Through the study he concluded that the Sycamore was deposited via gravity and/or turbidity currents. He concluded as well, through detailed faunal research, that the Sycamore was at the oldest middle Meramecian. Schwartzapfel (1990) and Franklin (2002) both supported this chronostratigraphic position as well. Coffey, 2000 later published a condensed version of this study concerning the lithostratigraphy, reservoir properties, and their relationships to reservoir performance in the Sycamore formation of the Carter-Knox field (Coffey, 2001). Using lithostratigraphy he broke the Sycamore section into 4 stratigraphic sections. Lastly Coffey, 2001 mentions the importance of post depositional fractures and their effects on reservoir enhancement within the Sycamore featured in the Carter-Knox field.

Franklin, 2002 published her master's thesis interpreting the depositional history of the Sycamore Limestone. Using samples from the I-35 roadcut outcrop she studied the unit via petrography, describing and interpreting the Sycamore to contain high amounts of silt in what she termed the silty peloidal wackestone lithofacies. She interprets the depositional setting as an

outer ramp to basin environment. She attributes the carbonate grains present in the unit to deep surface currents or bottom surface currents.

Interest in the Sycamore slowed once more during the early 2000's due to the modern technologic advances in unconventional reservoir development and the development of the unconventional giant, the Woodford Shale in Oklahoma. With the announcement of the STACK play in 2014 and its up-section Mississippian targets the Osage and Meramec formations, interest in the Mississippian units within the STACK and SCOOP has been reinvigorated. The difference though is that the Mississippian units are being viewed not as conventional but as potential unconventional reservoirs.

Several publications have been produced concerning the Mississippian aged Meramec formation (Duarte, 2018; Miller & Cullen, 2018; Milad, 2019; Terrell, 2019) and regional studies of Mississippian aged deposits are underway to understand how the Mississippian system in Oklahoma is related between the STACK and the SCOOP regions. One study that bridges the gap between the two areas is Miller & Cullen (2018). They correlate the Sycamore as a more distal unit that thickens to the south, referring to the sections of the Sycamore as benches, after Coffey (2001).

There is a great interest in the Sycamore formation as an unconventional unit. Various companies and institutions such as the STACK-Merge-SCOOP consortium at the University of Oklahoma have various projects underway to shed light onto the complexities of the Sycamore Formation and how to treat and utilize this unit as an unconventional reservoir rock.

2. GEOLOGICAL CONTEXT

2.1. Regional Geology

The Anadarko and adjacent Ardmore basins are located across central Oklahoma and south-central Oklahoma and spans for several hundreds of square miles. Close to this is the Ardmore Basin to the southeast beginning in Stephens county. The Ardmore Basin occupies Stephens, Carter, Marshall, Garvin Murray and Johnston counties. The Ardmore Basin followed the depositional axis of sedimentation of the Anadarko basin prior to deformation during the Pennsylvanian period.

The early history of tectonism in the present-day Anadarko basin region consisted of consolidation of the crust across Laurentia during the Precambrian, followed by the formation of a triple junction rift in southern Oklahoma between the late Precambrian to middle Cambrian (Franklin, 2002). The failed arm of the rift would have been what is now referred to as the Oklahoma Aulacogen. From the Cambrian to early Mississippian, the Oklahoma trough developed providing a principal axis of sedimentation parallel to the northwest to southeast trend of the aulacogen. The last major episode of tectonism occurred during the late Paleozoic as Gondwana approached Laurentia causing the Ouachita orogeny. This led to the uplift of the northwestern flank of the southern Oklahoma trough (Perry, 1988) to develop the asymmetric Anadarko basin, the Wichita orogeny (late Morrowan and early Atokan) (Johnson, 2008) generated the Wichita and Criner Hills uplifts that led to the development of the structurally complex Ardmore basin.

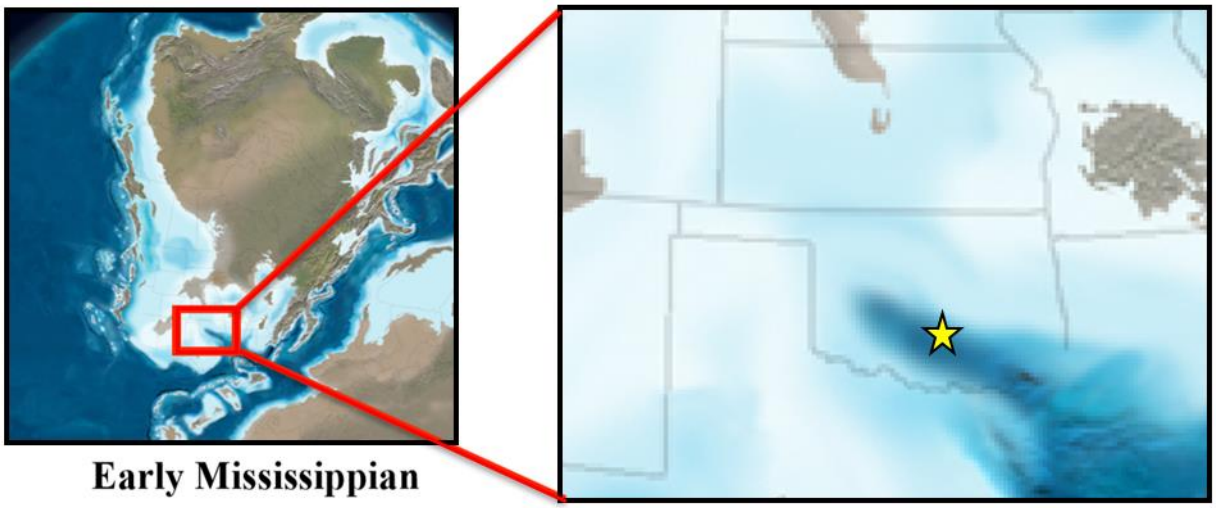

Figure 2: Paleogeographic map of the Middle Mississippian with a zoomed in map featuring the present day midcontinental region of North America including an outline of Oklahoma and surrounding states (Blakey, 2012). The yellow star represents the approximate area of this study.

2.2. Sycamore Formation

The Sycamore Formation overlies the Woodford Shale in southern Oklahoma as the distal portion of the Mississippian Meramec prograding clinoforms (Miller & Cullen, 2018). The Sycamore Formation extends into the Ardmore basin, which was once the southernmost end of the Anadarko basin. The southern Anadarko basin was isolated during the latest Mississippian and early Pennsylvanian by the Wichita-Criner Uplift. This event generated the Ardmore basin and the Criner Hills area, deforming up to the Mississippian and Pennsylvanian units.

The Sycamore Formation begins above the Woodford shale and contains several major intervals throughout the unit. The major intervals are commonly referred to as the Sycamore transition zone, lower Sycamore, middle Sycamore shale, middle Sycamore siltstone, upper Sycamore shale, upper Sycamore siltstone and is capped by the Caney Shale. Stratigraphically

the Woodford into the lower Sycamore transition zone marks the end of the transgressive systems tract of the late Devonian and begins a period of high stand systems tract across the present-day mid-continent.

The lowermost Sycamore is composed of a mixture of materials such as mudstone, shale, glauconites, and some sandy intervals. It is highly mixed and exhibits a serrated increasing upward API pattern on electric logs. The beginning of the lower Sycamore formation is considered to be a siltstone and exhibits a blocky gamma ray wireline log signature. This is due to the massive siltstone units present within this section. As will be mentioned in the methods and conclusions of this paper this section and the others appear with certain electric log characteristics but in reality, exhibit various features in core and hand sample that are too fine for the wireline tools to detect.

2.3. Area of Study

The immediate area of interest to this study pertains to the Sholem, Velma, and Tatums (Sho-Vel-Tum) fields in the northwestern Ardmore basin in which the X-1 well is situated. This area is located west of the Arbuckle Mountains. As previously mentioned is structurally complex, deformed by the "left-reverse transpressional tectonism in the Wichita thrust system and subsequent Arbuckle thrust system." (Perry, 1988). The Velma field is a structural trap caused by an anticlinal structure, generated during the Wichita uplift (figures 3& 4). The Velma fault is a reverse fault that generated an offset of several thousand feet in the location of the X-1 well. The well exhibits the Sycamore formation from near its base at 5,670 ft. to 5,130 ft. The deformation is responsible for offset beds to the west of the well and highly angled dipping beds

within the core. Several aspects of the deformation are important, 1. The Sycamore here was not subjected to the same depths of burial as the majority of the Ardmore basin. 2. The Sycamore formation in the Velma field may have undergone different subsurface processes than the Sycamore formation found to the north in the famous Carter – Knox field area.

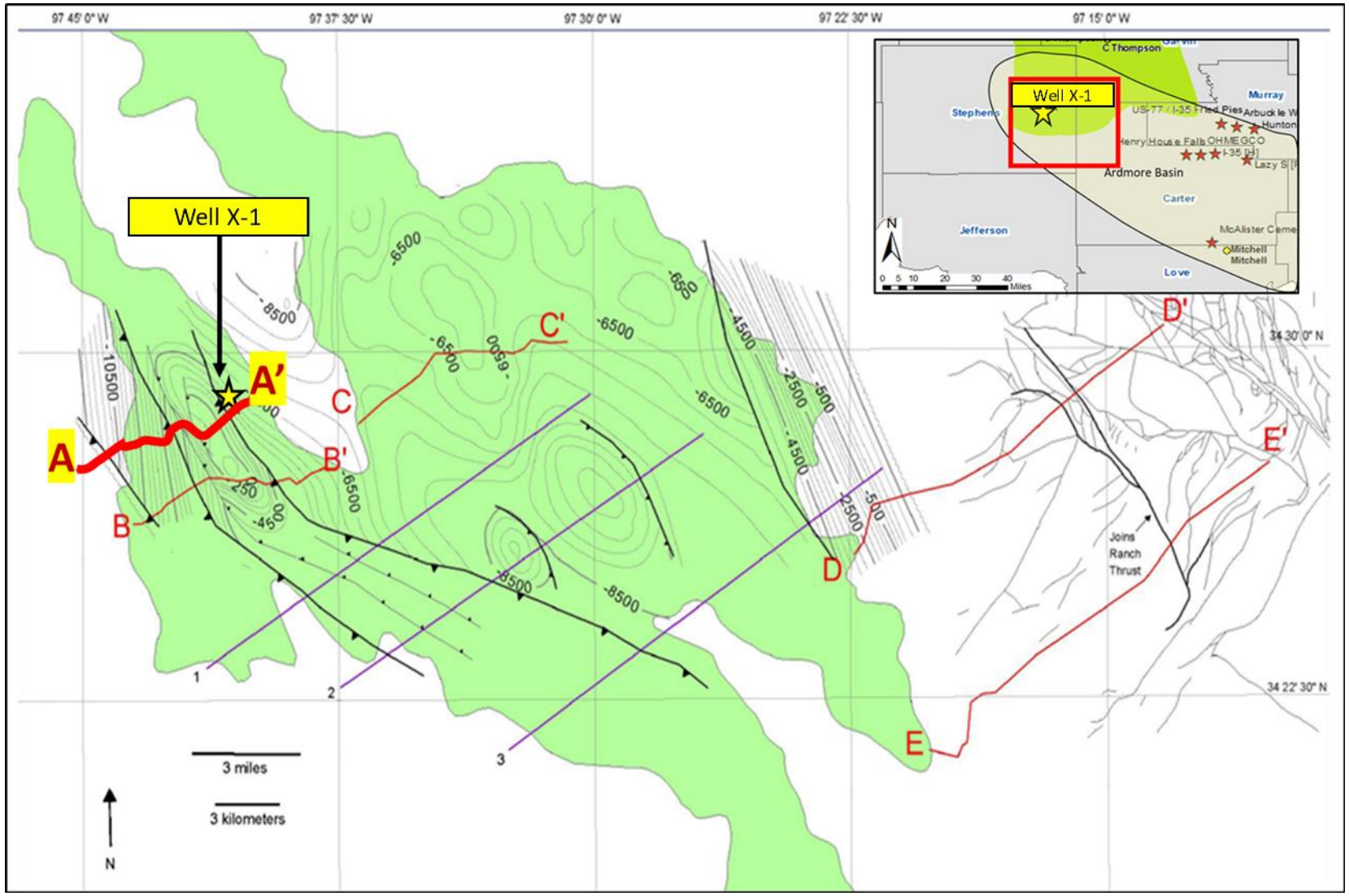

Figure 3: An isopach map of the top of the Sycamore formation the Sholem-Velma-Tatums (Sho-Vel-Tum) field (outlined in green) modified from Carpenter & Tapp (2014). The Velma field is the westernmost extension of the three fields and is in the major thrust faults. The cored well is marked by yellow star.

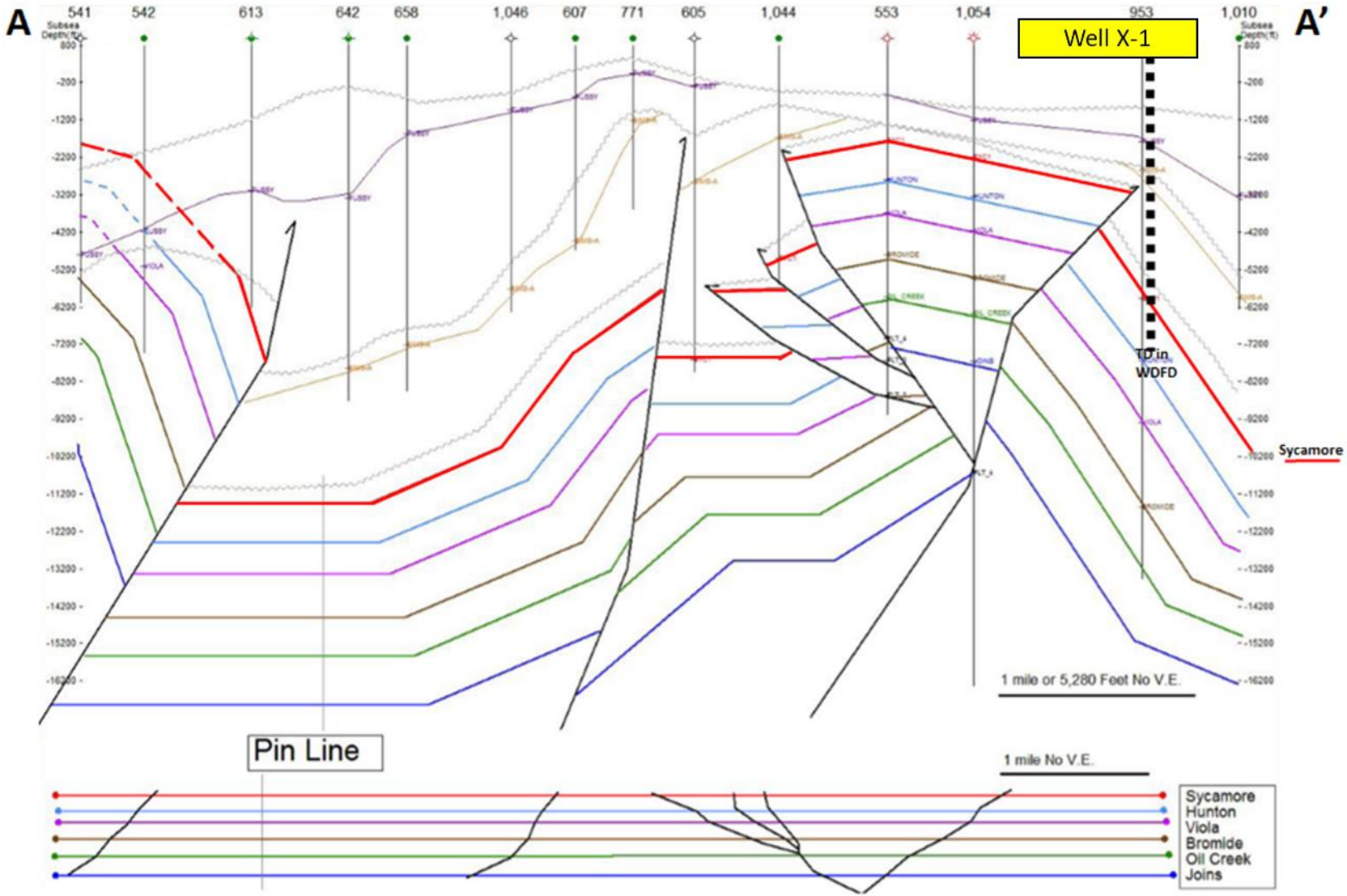

Figure 4: The balanced restored cross section of A- A' (from figure 3) modified from Carpenter & Tapp (2014). The anticline (left of the well) illustrates the complex structure of the Velma field from thrusting. The X-1 well is dashed to the east of the Velma reverse fault. The Sycamore formation top is marked in red.

The X-1 was drilled by Jones Drilling for the Getty Oil Company in 1980 targeting a conventional reservoir within the Sycamore Formation in the Velma field of eastern Stephens County. Unfortunately, the well was dry of hydrocarbons and even water to the extent that little water came up during the drill stem tests. Bedding in this location also exhibited highly angled dipping beds due to the thrust faulting in the Velma field. The well reached total depth (TD) at 5,700 ft at the Woodford shale and the kelly bushing (KB) was 8ft. The core was taken from 5,548-5,270 ft (5,540-5,262 ft. with KB) representing the upper transitional Sycamore, lower siltstone, middle shale, middle siltstone and most of the upper shale (Figure 5). Subdivision names of the Sycamore followed those of Milad, 2019. Sections not featured in this core are the lowermost transition zone and the upper Sycamore, although they can be seen in the wireline logs and were correlated to nearby wells.

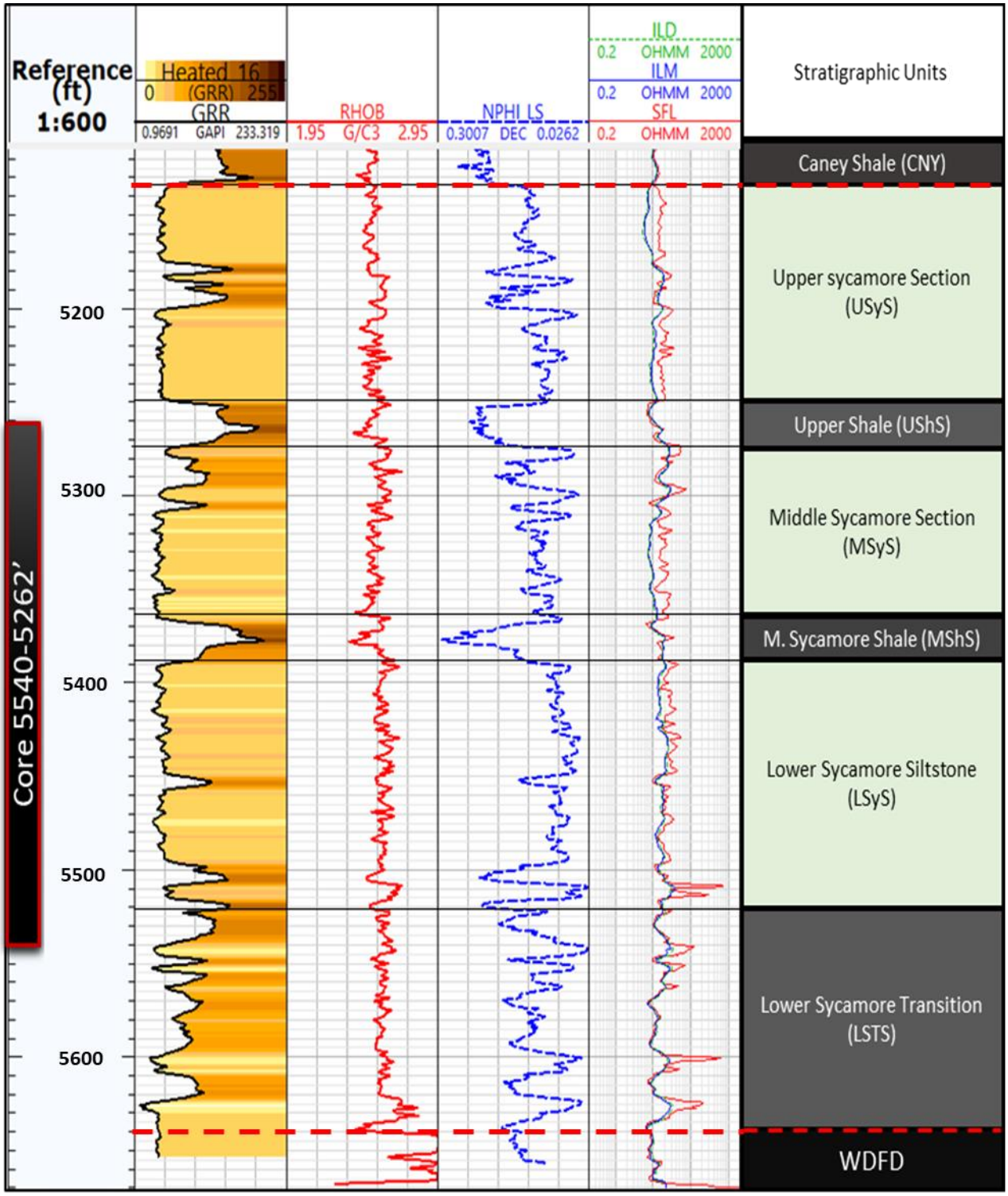

Figure 5: Outline of the stratigraphic units featured in the X-1 well and location of the core relative to the gamma ray log (GRR), porosity & permeability logs and naming scheme for the intraformational intervals found within the Sycamore.

3. METHODOLOGY

3.1. Lithofacies Identification

3.1.1. Core Analyses

Lithofacies identification for the Sycamore Formation in the X-1 began with core analysis. For proprietary reasons a generic well name was given (X-1) and well depths were shifted in this report but maintain original thicknesses. The base of the core was marked at 5,548 ft and topped out at 5,270 ft core depth. Bedding orientations exhibited in the core appear low angled to highly dipping due to inconsistent slabbing. An offset of -8 ft was calculated to align the core with the electric logs, but the core depth will be used when describing the samples throughout this thesis. The 278 ft core was marked at a two-inch interval to note data collection points and a core description was completed at a 6 ft interval. Later description was provided at a 1ft interval when generating a stratigraphic column. Features observed and noted included grain size (vf sand to clay), bedding features such as soft sediment deformation, grading features, fractures, healed fractures, identification of trace fossils, bedding terminations, sedimentary structures, and effervescence. A fracture analysis was not conducted because of the irregular slabbing of the core and the dramatically tilted beds. The analyzed features are important in that their qualities can be telling of depositional history.

An important element considered while evaluating the core was ichnofacies. The Sycamore Formation through most of the core, exhibited varying degrees of bioturbation. The importance of this comes into mind when considering the destruction of primary sedimentary fabrics, the environmental implications of the presence and abundance of various taxa, and the enhancement or destruction of porosity and permeability caused by resultant ichnofabrics.

Baniak et al., 2015 speaks to the enhancement of reservoir porosity and permeability possible in ichnofabrics. Presences of the various burrows were identified throughout the core and suggest certain environmental conditions. Following the methods of Lazar et al. (2015) a Bioturbation Index (BI) score of 0-5 was used to measure the various degrees of bioturbation throughout the core (see Table 1).

Bioturbation Index, BI	Verbal BI	Description
0	Not bioturbated	No visible burrows; original sedimentary structures preserved
1	Weakly bioturbated	Continuous beds, some burrows
2	Sparsely bioturbated	Discontinuous beds; some burrows
3	Moderately bioturbated	Remnant bedding, common burrows, individual burrows mostly recognizable
4	Strongly bioturbated	Minimal bed continuity, abundant burrows, some distinct burrows
5	Churned	No remnant bedding, fully homogenized, hard to recognize individual burrows

Table 1: Ranking of Bioturbation Index (BI) used during core analysis. Modified after Lazar et al. (2015) (after Reineck 1963, Potter et al. 1980, Droser and Bottjer 1986, Taylor and Goldring 1993, and Aplin and Macquaker 2010).

3.1.2. Chemostratigraphic Analysis

A chemostratigraphic analysis was conducted to observe qualitative elemental compositions of the Sycamore Formation. The core was marked at a two-inch interval designating depths along the core that would serve as locations of both Major and Trace elemental analyses. Data was collected using a Bruker Traces IV-SD handheld X-ray

fluorescence (HHXRF) spectrometer. Major elements were measured for 90 seconds at 15 kV accelerating voltage, 35 mA under vacuum. Trace elements were measured under 60 second scanning intervals at 40 kV accelerating voltage, 17 mA with a Ti-Al filter at atmospheric pressure.

Data from both major and trace analyses were converted to parts per million (ppm) via the mudrock parameters prescribed by Rowe et al. (2012a). A total of 30 elements were measured by the XRF but only 13 were used for the bulk of this study. In grouping elemental abundances (i.e. Ca, Mg, & Sr; see table 2) we can look at relative composition of the rock from base to top of the core and compare the various elemental proxy groups, reflecting carbonate, clay, continental, and deep marine anoxic environmental proxies.

Environmental Proxy	Paleoenvironmental Interpretation
Calcium (Ca)	Carbonate source
Strontium (Sr)	Carbonate source
Magnesium (Mg)	Dolomite source
Aluminum (Al)	Clay minerals & feldspars
Potassium (K)	Clay minerals & feldspars
Silica/Aluminum (Si/Al)	Quartz
Titanium (Ti)	Continentally derived
Zirconium (Zr)	Continentally derived
Molybdenum (Mo)	Bottom water anoxia
Phosphorous (P)	Organic origin (?)

Table 2: XRF Elemental proxies and their corresponding origins (table modified from Duarte-Coronado, 2018).

3.1.3. Mineralogical Modeling Using Elemental Data

Mineralogy is commonly analyzed using X-ray diffraction but due to the generally high cost to analyze samples, attempts have been made to model mineralogies using XRF derived data. A mineralogical model was made using methods of previous authors (Ratcliffe, 2010; Wright et al., 2010; Stilwell et al., 2013; Thruston & Taylor, 2016; Ruppel et al., 2017). The model uses "empirically obtained linear regressions, highly dependent on the mineral associations present in each formation" (Becerra, 2017), to generate mineral models reflecting bulk mineralogies for siliciclastic, carbonate, and clay mineralogies.

The calculations used in this thesis follow the Normalized Si-Al+K+Ti+Rb-Ca+Sr+M+Mn concentrations calculation prescribed in Becerra (2017). The Si abundance according to Becerra (2017) was found to be related to quartz in a correlation matrix. This was followed by the association of Al, K, Ti, and Rb for clay minerals. And positive correlations for the carbonate mineralogies using Ca, Sr, Mg, and Mn. The Calculations are featured below.

$$Total = Si + Al + Ti + K + Rb + Ca + Sr + Mg + Mn \quad (1)$$

$$Quartz\ \% = \frac{(Si)*100}{Total} \quad (2)$$

$$Clays\ \% = \frac{(Al+K+Ti+Rb)*100}{Total} \quad (3)$$

$$Carbonates\ \% = \frac{(Ca+Sr+Mg+Mn)*100}{Total} \quad (4)$$

The second approach to calculating mineralogies was derived from observing three major end member compositions that are common in marine deposits, SiO2 – Al2O3*5 – CaO*2, derived by Brumsack (1989). Based on this approach concentrations of Si, Al, and Ca were first converted to molecular weight percent and then to oxides (SiO2, Al2O3*5, & CaO*2) using the equations (equations 5, 6, & 8) from Brumsack (1989). A total for the oxides was calculated in equation 8 and lastly mineral compositions were calculated and normalized (100%) using the equations 9, 10, & 11.

$$SiO2 = \frac{((Si\%)*60.084)}{28.086} \quad (5)$$

$$Al2O3 = \frac{(Al\%)*101.961}{26.892} \quad (6)$$

$$CaO = \frac{(Ca\%)*56.077}{40.078} \quad (7)$$

$$Total = Sio2 + \ (5 * Al2O3) + (2 * CaO) \quad (8)$$

$$Quartz\ \% = \frac{(SiO2)*100}{Total} \quad (9)$$

$$Clays\ \% = \frac{(5*Al2O3)*100}{Total} \quad (10)$$

$$Carbonates\ \% = \frac{(2*CaO)*100}{Total} \quad (11)$$

3.1.4. X-ray Diffraction

X-ray diffraction was conducted on 17 crushed rock samples to analyze for bulk mineralogy using the Brags Brintano methodology. One gram of material from each sample was placed in a micronizer canister with ceramic beads and 5-7 ml of methanol to serve as a lubricant in the micronizing process. The canister was loaded into the micronizer and run for 5 minutes to ensure uniform pulverization of the rock materials. Samples were dried and then sieved (4-micron mesh) over glass slides. Removal of the excess material was done using a blade, carefully as to not preferentially orient the grains. Powdered samples were then loaded into a Rigaku Ultima IV diffractometer to run analyses.

The resultant data was reviewed using the MDI Jade 2010 system for XRD analysis. The program aided in matching mineralogies to the resultant curves. This data serves as a quantitative analysis of the rock samples to provide greater insight into the mineralogies of the different lithofacies of the Sycamore Formation. Following the ascribed mineralogical identification from Moore & Reynolds (1997) the results of the XRD were interpreted.

3.1.5. Brittleness Index

Rock hardness was measured every two inches of the core using an Equotip Picolo2 rebound hammer. The test measures the hardness based on the rebound of a tungsten carbide ball (3mm) following impact of 11Nmm applied by spring force on a flat sample surface (Becerra et. al, 2018, & Leeb, 1979). The resultant hardness (LH) value is a ratio of rebound velocity (Vr) to impact velocity (Vi) (Leeb, 1979). Five tests were conducted at each XRF measurement point on

the core and their results were averaged. The LH was measured at 1,668 locations that correspond to the XRF sample locations throughout the core. This set of rock hardness measurements was added to the overall evaluation of rock properties and chemostratigraphy.

3.1.6. Petrographic Analysis

17 core plugs were taken from the X-1 well core and thin sections of each plug was generously provided by 89 Energy. The petrographic investigation was conducted using a Zeiss AxioImager Z1TM petrographic microscope. Standard procedures such as observance through plain polarized light and cross polarized light were followed to identify constituents such as texture, composition, primary, secondary constituents, cementation, and grain characteristics in thin section. Reflected light was used to observe opaque minerals. Thin sections were processed with blue epoxy stain to view pore spaces and red alizarin dye was also used to stain calcite. Oil was placed on the slides along with glass cover slips. The investigation included observance of various minerals present and lithologic names were given based on composition and fabric. Previous lithofacies names were integrated in the naming process.

3.1.7. Rock Eval and TOC Analyses

Rock-Eval pyrolysis (S1, S2, S3, & T-max) and Total Organic Content (TOC) were measured by Weatherford Laboratories from 10 core plug samples (table 3) from more argillaceous sections. The samples are labeled C-1, C-2, C-3, C-5, C-10, C-11, C-15, C-16, and C-17. The results were used to observe the organic content of mudstone sections of the core and

evaluate the internal hydrocarbon generation potential of the Sycamore in this area. Total Organic Carbon (TOC), residual hydrocarbon content (S1; oil & gas), remaining viable organic content (S2), and non-productive carbon (S3) were measured and used in this evaluation.

Sample	TOC	S1	S2	S3	Tmax (°C)	HI	OI	S2/S3	S1/TOC*100
C-1	12.55	3.8	68.88	1.16	432	548.84	9.24	59.38	30.28
C-2	1.097	0.5	3.61	0.42	433	329.08	38.29	8.60	47.40
C-3	1.11	0.6	4.51	0.43	433	406.31	38.74	10.49	49.55
C-5	2.525	1.1	13.32	0.48	436	527.52	19.01	27.75	43.96
C-6	0.798	——	——	——	——	——	——	——	——
C-10	2.05	0.9	7.83	0.28	431	381.95	13.66	27.96	43.90
C-11	1.075	0.5	4.91	0.49	434	456.74	45.58	10.02	43.72
C-15	4.295	1.6	24.21	0.34	437	563.68	7.92	71.21	37.02
C-16	2.305	0.9	11.64	0.35	435	504.99	15.18	33.26	38.61
C-17	1.06	0.6	4.36	0.53	435	411.32	50.00	8.23	51.89

Table 3: Rock Eval and TOC results.

3.1.8. Porosity & Permeability

Porosity and permeability were measured by Weatherford Laboratories as well, using 15 of the thin sectioned samples. Measurements taken observed permeability to air (mD), permeability to klinkenberg (mD), ambient porosity (%), porosity NCS (%), and grain density (gm/cc) (table 4).

Sample ID	Permeability to Air (mD)	Permeability to Klinkenberg (mD)	Porosity Ambient (%)	Porosity NCS (%)	Grain Density (gm/cc)
C-1	———	———	———	———	———
C-2	0.015	0.0061	7	6.9	2.66
C-3	0.244	0.161	8	7.9	2.68
C-4	0.0006	0.0001	3	3	2.67
C-5	0.151	0.093	6.2	6.2	2.63
C-6	0.022	0.0095	5.3	5.2	2.71
C-7	0.011	0.0039	8.3	8.3	2.71
C-8	0.145	0.089	12.5	12.3	2.68
C-9	0.152	0.094	14.8	14.7	2.65
C-10	———	———	———	———	———
C-11	0.067	0.036	4.3	4.2	2.67
C-12	0.002	0.0004	2.9	2.7	2.68
C-13	0.013	0.0047	6.5	6.4	2.67
C-14	0.016	0.0064	5.8	5.7	2.67
C-15	———	———	4.3	———	2.45
C-16	———	———	3.9	———	2.59
C-17	———	———	3.9	3.7	2.65

Table 4: Core plug porosity and permeability results.

3.2. Stratigraphic Framework

3.2.1. Well-log Analysis & Correlation

Basic well-log analysis was used to observe characteristics of the X-1 well and to correlate the well to nearby wells. Coffey (2001) presents the Fox Alliance #5 well as a type log and discusses the various sections of Sycamore deposits observed. Major lithostratigraphic sections of the Sycamore were correlated in the X-1 based on Coffey's 2001 lithostratigraphic sections from his study of wells in the Carter-Knox field. From here nearby wells in the Sholem

and Tatums fields were correlated along with a correlation of the gamma ray profile taken by Benmadi Milad on the I-35 roadside outcrop (Milad, 2019).

3.2.2. Sequence Stratigraphic Correlation

The Sycamore formation is a mixed siliciclastic -carbonate system with several argillaceous shale intervals. It overlies the Woodford shale and is overlain by the Caney Shale. These two major shales are considered to represent transgressive systems tracts. Moving up from Woodford into the lowermost Sycamore, the composition of the rock material changes drastically into a calcified siltstone. This has been interpreted as belonging to the start of a high stand systems tract (HST). The Sycamore Formation represents an overall HST and has even been interpreted to be of a prograding clinoformal form (Miller & Cullen, 2018).

The second order sequence stratigraphic cyclicity is composed of 3rd, 4th, and 5th order parasequences observed by wireline electric logs (figure 6). Three color coded arrows were used to represent ideas of the log characteristics; Red indicates a lowering of gamma log signature or possible coarsening of material, black represents relatively straight log signature or relatively stable input of material, and green indicates a rise in log signature or ‘dirtying’ upward. These three signature types can be used to observe changes in deposition that support the argument of varying internal stratigraphy in the Sycamore.

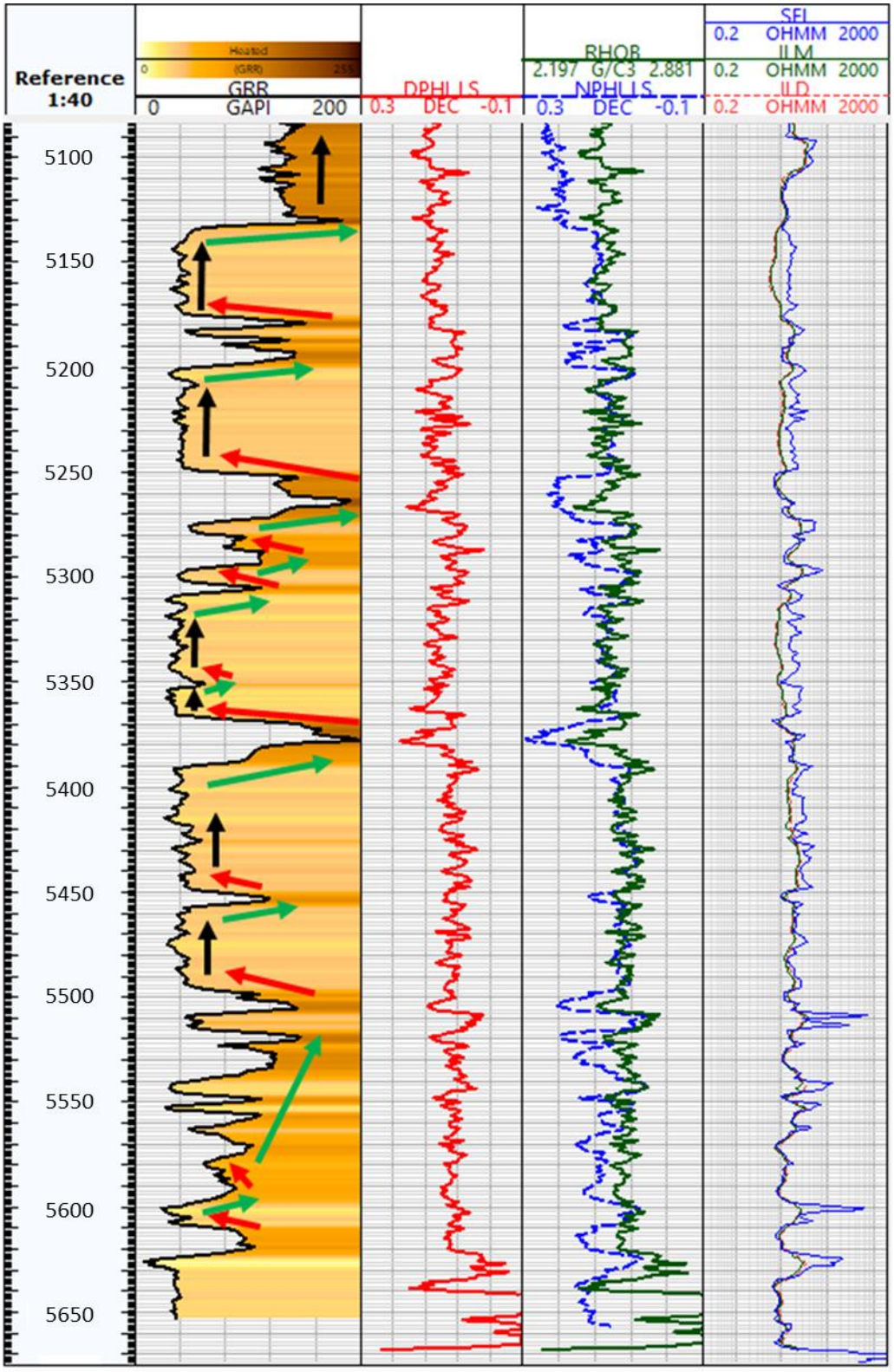

Figure 6: Gamma ray log with arrows indicating changes in sedimentation. Green indicates a dirtying upward, red a cleaning upward, and black a period of relative continuous sedimentary material.

3.3. Chemofacies Classification

3.3.1. XRF data-Conditioning

XRF elemental measurements considered for the Multivariate Cluster Analysis (MVCA) consisted of Ca, Mg, Sr, Al, K, Th, Zr, Ti, Mo, V, S, P, U, Si/Al ratio, and the Si/Ti ratio. These elements were chosen based on their geologic significance and use in the chemostratigraphy section. The measurements were prepared and entered into an excel based statistical software, XLSTAT 2018, to conduct the hierarchical cluster analyses (HCA) and generate an elbow curve (figure 7) to determine the optimal number of clusters.

3.3.2. Multi-variate Clustering Analysis (MVCA)

The multivariate cluster analyses were used to generate chemofacies. Chemofacies are units that share geochemical similarities based on a hierarchical system. “The hierarchical cluster analysis (HCA) calculated the chemical similarity within the groups using a Euclidian distance to a cluster’s centroid. The centroid of newly grouped clusters was calculated using the minimum variance of the original cluster, known as Ward’s Method (Ward, 1963).” (Turner et al., 2015).

The optimal number of clusters for this analysis was 7 according to the Elbow curve (figure 7). The range of clusters with minimal variance is between 7 to 10 clusters. Although ten lithofacies were identified via core description and petrography, 7 clusters were used for the chemofacies because the range of variance in figure 7 does not reflect much change after 7 classes. Also limiting the number of clusters prevents redundancy within the chemofacies allowing the 10 lithofacies to be upscaled. Chemically the three dominant groups of lithofacies,

mudstones, siltstones, and calcified siltstones, would likely exhibit features that grouped them more closely than the 10 lithofacies which were named incorporating qualifiers (i.e. laminated, bioturbated, etc.).

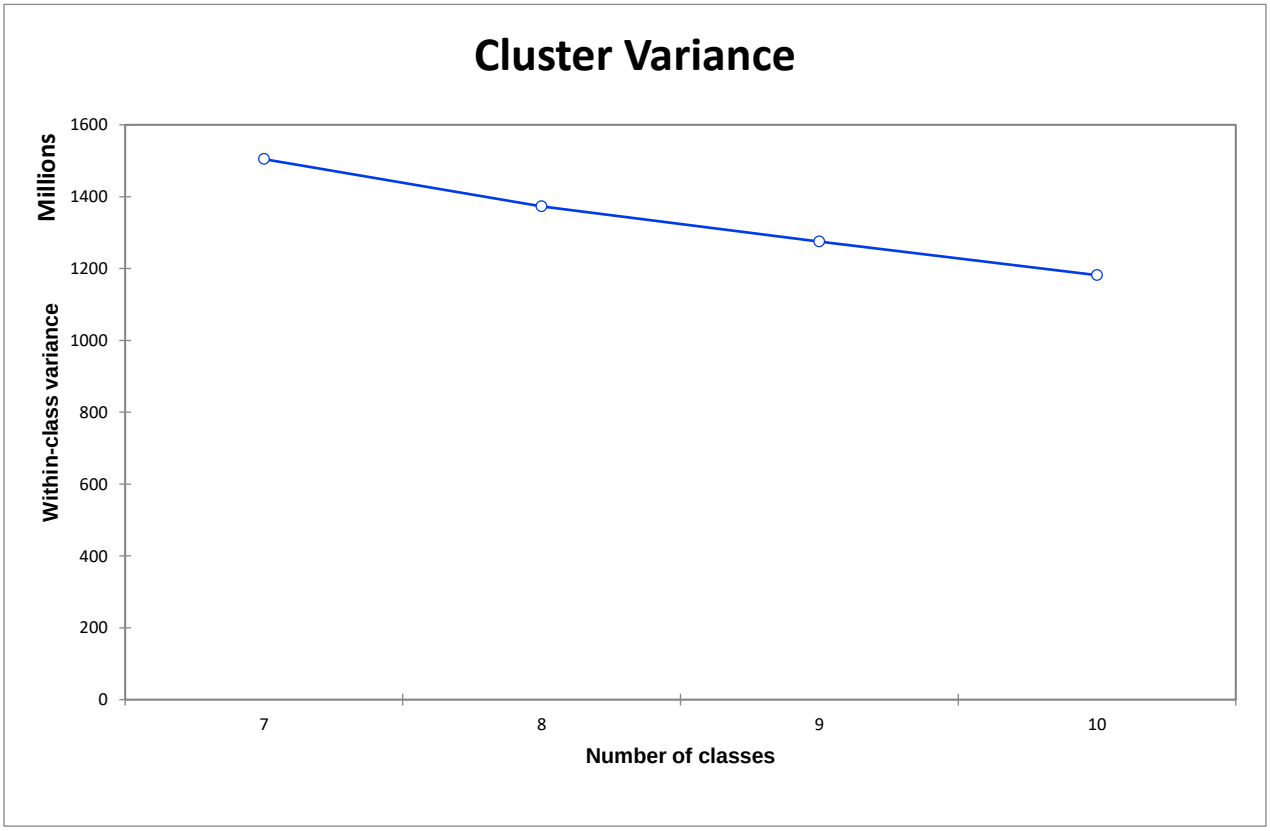

Figure 7: The optimal number of clusters ranged from 7 to 10. The number of clusters chosen for the MVCA for the Sycamore was 7 because the variance beyond 7 is minimal. This is less than the number of lithofacies (10) because the lithofacies qualifiers (laminated, bioturbated, etc.) may not necessarily be distinguishable via chemofacies.

4. RESULTS & DISCUSSION

4.1. Lithofacies

Mentioned within the previous section are the lithofacies identified within the core. Lithofacies were identified primarily from core observation and further defined using several additional types of data including petrography, XRF, and XRD. Two major groups of facies types were identified as the dominant rock type, group 1 mudstones and group 2 siltstones. From here qualifiers were added to distinguish other reoccurring properties that were thematic to each lithofacies. These included the presence of laminations, bioturbation, and noticeable calcite cementation. To be noted is the angles of dip featured in core photos vary greatly due to inconsistent slabbing of the core. The well was drilled over the footwall of the reverse fault (figures 3 & 4) and bedding planes in the core feature highly dipping beds. They also exhibit discontinuous angles of the bedding planes due to a poor slabbing job.

The lower to middle Sycamore Formation in the Velma field is composed of ten (10) lithofacies recognized from the X-1 well. They consist of the following: (1) Laminated Mudstone (LMdst), (2) Bioturbated Mudstone (BMdst), (3) Laminated Bioturbated Mudstone (LBMdst), (4) Massive Siltstone (MSt), (5) Laminated Siltstone (LSt), (6) Bioturbated Siltstone(BSt), (7) Laminated Bioturbated Siltstone (LBSt), (8) Massive Calcite cemented Siltstone (MCcSt), (9) Bioturbated Calcite Cemented Siltstone (BCcSt), and (10) Interbedded Siltstone (ISt). Table 5 outlines the lithofacies, their main qualifications, and interpreted depositional processes.

Lithofacies ID	Code #	Lithofacies	Description	Interpretation
LMdst	1	Laminated Mudstone	Fabric dominated by parallel to sub-parallel laminations, darker in color, may be bioturbated	Quiet deepwater setting in which finest and hemipelagic materials settled.
BMdst	2	Bioturbated Mudstone	Burrow dominated fabric, may be faintly laminated	Quiet deepwater setting in which organisms were able to inhibit, favorable conditions for the zoophycos ichnofacies
LBMdst	3	Laminated Bioturbated Mudstone	Mudstone in composition featuring laminations as well as burrows, BI>1	Series of low energy environment during which laminations occur via settling of suspended sediments. Water chemistry, temperature, and sediment supply stable enough for burrowing organisms to thrive.
MSt	4	Massive Siltstone	Massive, no visible sedimentary structures, silty, low effervescence	Gravity flow or turbidity deposit, deposited at once and in massive or thick sequences (Bouma A), possible amalgamation of deposits.
LSt	5	Laminated Siltstone	Laminated siltstone	Deposited under laminar flow regime, sometimes overlying the MSt sections (Bouma B)
BSt	6	Bioturbated Siltstone	Burrows present in samples, low effervescence	Uppermost section of a massive siltstone deposit in which burrowing organisms extended, or prolonged periods of silt and carbonate grain sedimentation which allowed for inhabitation by limited species.
LBSt	7	Laminated Bioturbated Siltstone	Siltstone facies exhibiting both laminations and a BI>1, has varying amounts of argillaceous material	Stable sediment supply where burrowing organism present in thicker successions,
MCcSt	8	Massive Calcite Cemented Siltstone	Massive looking siltstone, vigorous effervescence, lightest gray color in the core, vertical fractures	Gravity flow or turbidity deposit (Bouma A), deposited at once and in massive or thick sequences with higher concentrations of carbonate materials and preferentially cemented with calcite.
BCcSt	9	Bioturbated Calcite Cemented Siltstone	Calcite cemented siltstone with burrows present	Uppermost sections of massive deposits burrowed into by organisms between depositional episodes of carbonate and silt material.
ISt	10	Interbedded Siltstone	Alternating siltstones and mudstones within a narrow interval (<1')	Alternating episodes of silt with carbonate deposition to more argillaceous or hemipelagic deposition. Deposited via slow sedimentation in deep-sea environments from nepheloid layers (Boggs, 1995).

Table 5: Summary of the lithofacies identified in the Lower Sycamore Transition zone to the Upper Sycamore Shaley section. Lithofacies code numbers are featured in figure 8.

4.1.1. Laminated Mudstone

The laminated mudstones present in the Sycamore Formation are found in the lower transitional zone, middle shaley section, and upper shaley section, and in many minor intervals in the silt dominated sections. This lithofacies was identified based on first core observations then further characterized via petrography, XRF, and XRD (figure 8). This facies is highly argillaceous and breaks along laminations. Laminations are parallel planar and in hand sample the material is the darkest of the core and looks chocolatey. In thin section the material is dominated by clay mineral matrix (>30%) but still contains some siliciclastic material although in significantly lesser amounts than in other facies (<60%). Carbonate mineralogies are minimal in this facies (<5%) and heavy minerals are present in the form of pyrite and several other undistinguished oxides.

Silt grains present in this sample are angular and of 60 microns to 4 microns in size. Clay minerals dominate the sample, with XRD results revealing greater than 30% of the rock composition as phyllosilicate minerals. The tectosilicate abundance ranges between 54-56% within the tested samples. Carbonate content is relatively low with a maximum of 9.8%, and additional minerals account for 6% or less within each of the samples (table 6). Samples C-1, C-10, and C-15 were noted as Laminated Mudstones in core observation and match this lithofacies in thin section.

The depositional interpretation for Laminated Mudstones is that of lesser order (unlike the major Woodford shale) than major mud transgressional facies tract during which time clay rich, very fine silt, and organic material settled out of suspension as a hemipelagic mud on the

ocean floor or in some cases as hyperpycnites (Slatt, 2013). Several feet of accumulated material would imply a longer period of clay rich sedimentation and less detrital input.

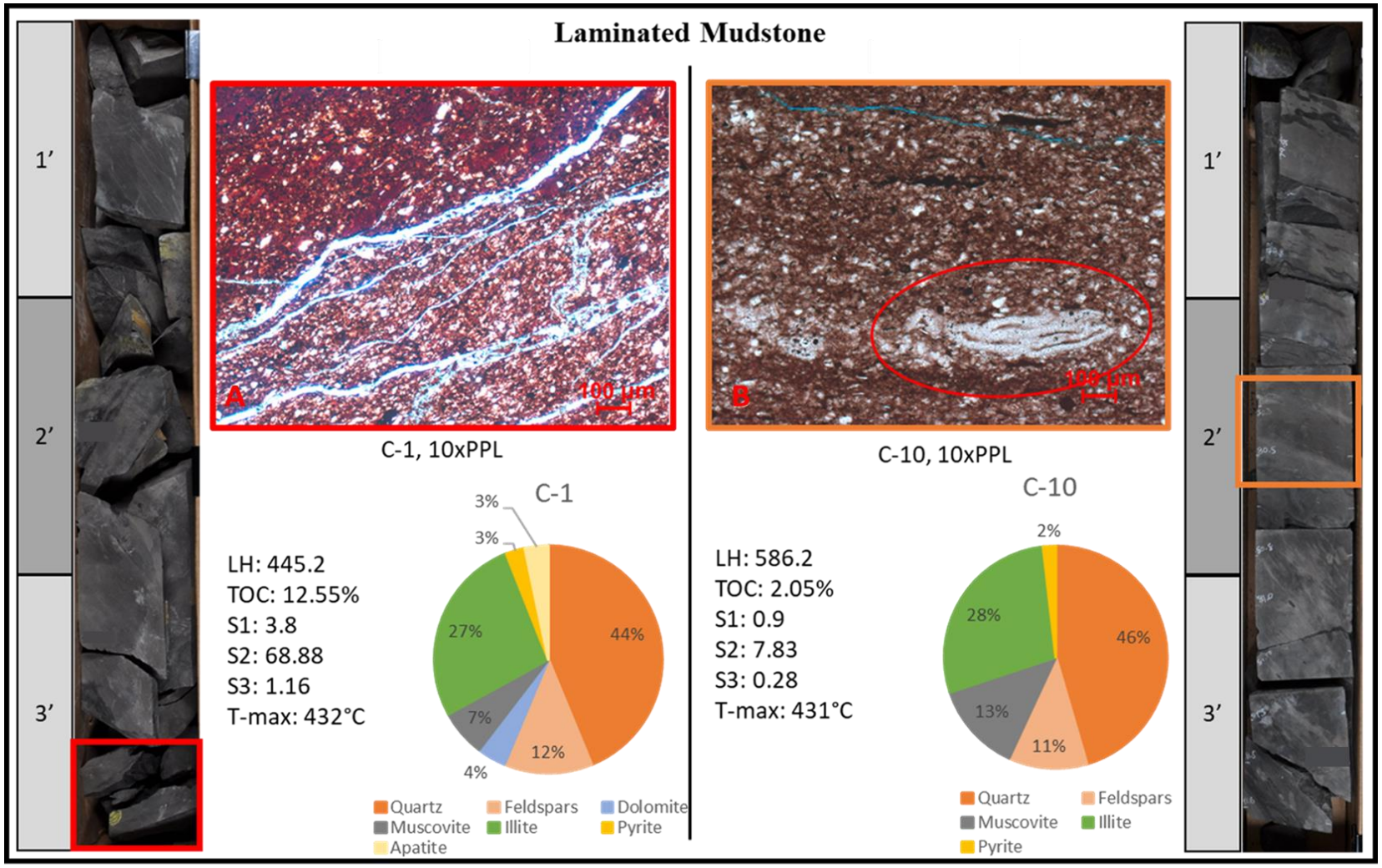

Figure 8: Laminated Mudstone lithofacies in core and thin-section compared to XRD mineralogical composition. In sample C-1 the mudstone exhibits lamination and openings which may look like fractures but are from the thin sectioning process. The Leeb hardness (LH) of 445 is low compared to the hardness of other lithofacies. The C-10 sample shows laminated argillaceous material and angular quartz grains thought to be detrital in origin (Schieber, 2009; after Blatt, 1992 and Schieber, 2000). The feature circled is identified as a collapsed agglutinated benthic foraminifera.

4.1.2. Bioturbated Mudstone

The bioturbated mudstone facies exhibits bioturbation greater than 1 on the bioturbation index and a more argillaceous composition than the siltstones. This lithofacies was identified in core by the lack of visible lamination and typically heavier bioturbation (BI of 3-5) (figure 9). It is interpreted to be deposited during quiet calm periods in a marginal marine setting during which there is oxygen in the system.

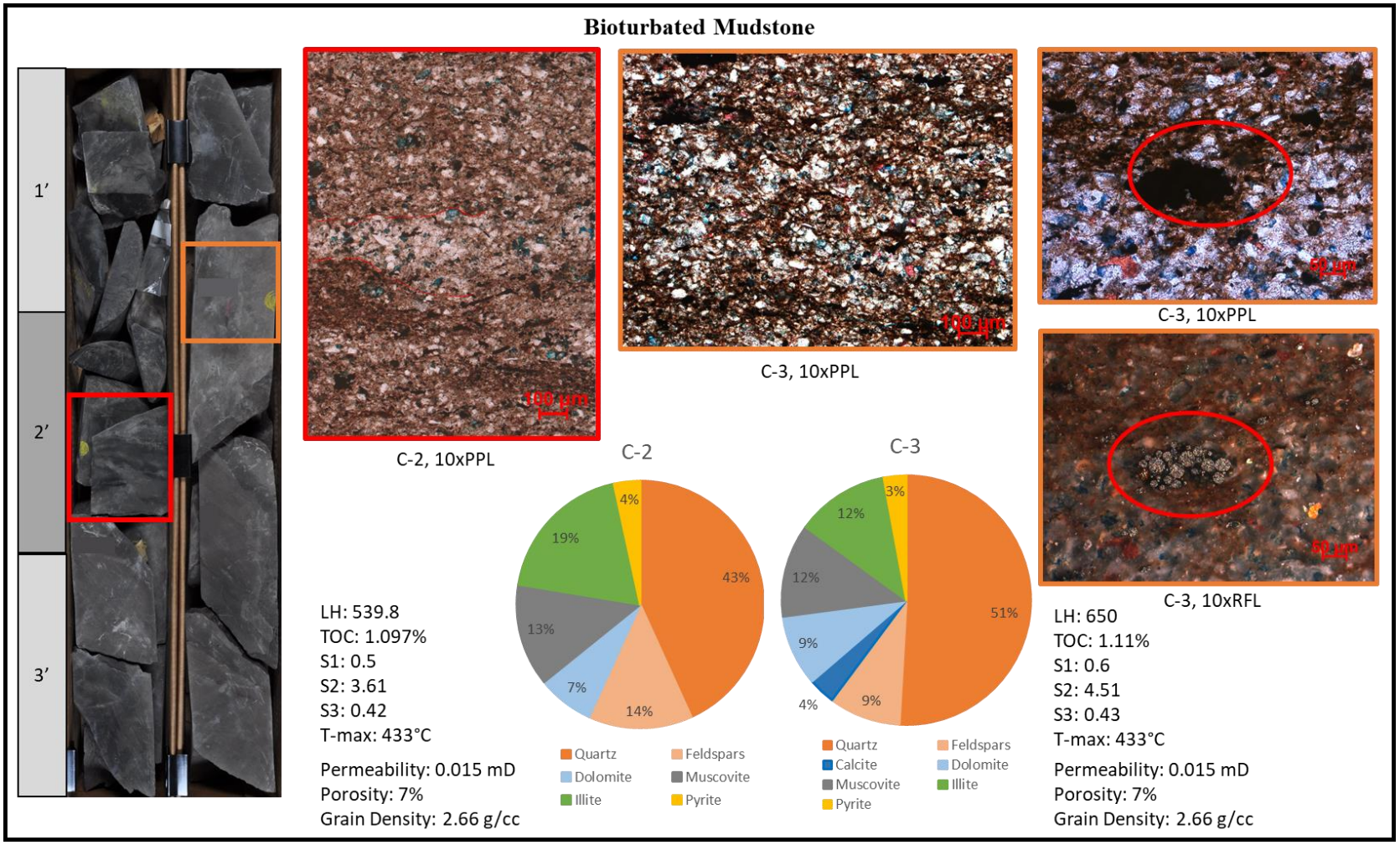

Figure 9: Bioturbated mudstone lithofacies represented by the C-2 and C-3 samples exhibits burrows in hand sample that are particularly distinguishable when the core is wet. Laminations are faint and burros can easily be found with a bioturbation index of >2. The hardness of this lithofacies is lower resembling that of a mudstone. Where the material is more quartz driven (C-3) the hardness increases. Angular quartz grains are present in these samples along with some lamina of siliciclastic grains (outlined in C-2 photomicrograph). Burrows seem to concentrate quartz grains and flocculate clays (C-2 and C-3). In C-3 two photos (far right) exhibit pyrite spherules in plane and reflected light. These are indicative of early diagenesis.

4.1.3. Laminated Bioturbated Mudstone

Laminated Bioturbated Mudstones are distinguished by their darker color, often near richer laminated mudstone sections, with visible laminations and burrows that are present and/or nearly destroy the primary sedimentary fabric (BI>2). The thin section C-17 represents this facies and exhibits some accumulations of argillaceous material and of silt grains (figure 10). The concentrated argillaceous material appears to be planar in some instances, and eye shaped or channeled in others with silt grains collected nearby. Calcite is present in the sample but does not control the matrix or cement. Mineralogically, the sample contains 48.9% silt and feldspars, 24.5% carbonate material, 24.3% clay material and 2.4% additional minerals such as pyrite.

This lithofacies is representative of a transgressive systems tract with a steady rate of sedimentation. Siltstone lithofacies grade up into the laminated bioturbated mudstones implying a transition from mixed clastic-carbonate deposition into a quieter or possibly deeper setting from which suspended argillaceous materials settled. The presence of burrows is indicative of a more stable time of deposition in which organisms could comfortably inhabit the sediment. The lithofacies is of the Cruziana ichnofacies, evident by the presence of Teichichnus, Phycosiphon, and other visible but undistinguished burrows.

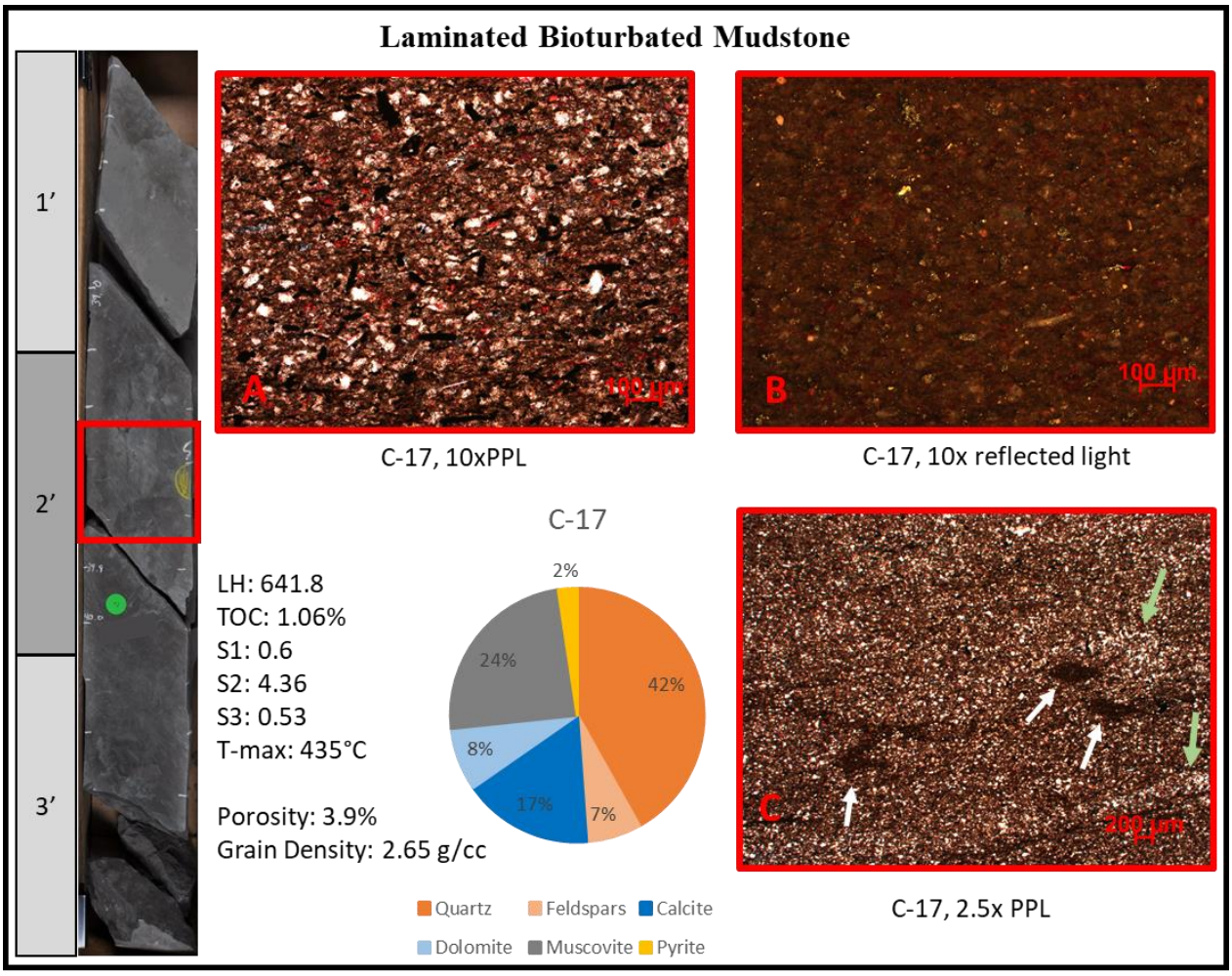

Figure 10: The laminated bioturbated mudstone lithofacies represented by the C-17 sample. Thin section images are outlined in red corresponding to the location in the red box over the core image. Thin section images A and B were taken in plane and reflected light at 10x magnification. A shows the angular sized silt grains and opaque martials in a dominantly clay matrix, reflected by the XRD clay mineralogy. There is 17% calcite within this sample which is intergranular and seems to be secondary. Thin section image B was taken at 10x magnification and illustrates the pyrite (golden color) within the sample. Thin section image C was taken at 2.5x magnification in plane polarized light. It illustrates clay floccules (white arrows) and silicate grain floccules (green arrows) around them. These are interpreted to be the burrows previously observed in hand sample.

4.1.4. Massive Siltstone

Massive siltstone sections are identified as lacking in sedimentary structure, lacking in bioturbation (BI:0), contain silt material that is not visible other than under microscope, and contain minimal argillaceous material. These sections dominate the lower and middle silt-based sections of the core, have a weak or delayed effervescence to 10% hydrochloric acid when compared to the vigorous reaction observed in a calcite cemented section (figure 11). The mineralogy as confirmed by XRD showed the sample C-8 is composed of 46.2% tectosilicates, 50.1% carbonate material, 3.7% phyllosilicates and 0% additional mineralogies. The lithofacies is represented by the C-8 thin section and XRD results.

Within the lower and middle silt sections, massive siltstone sections can be found with a 2 - 6-inch section of overlying bioturbated siltstone and a hemipelagic layer of mud often bioturbated as well. The section is interpreted to be more of a gravity or density flow, as in sections within the middle Sycamore silty section there are flame structures over the hemipelagic or laminated mud layer. When describing the unit as part of a Bouma Sequence it would be considered a Bouma A section for its massiveness and eventual fining upward character. Bouma C features were sometimes present.

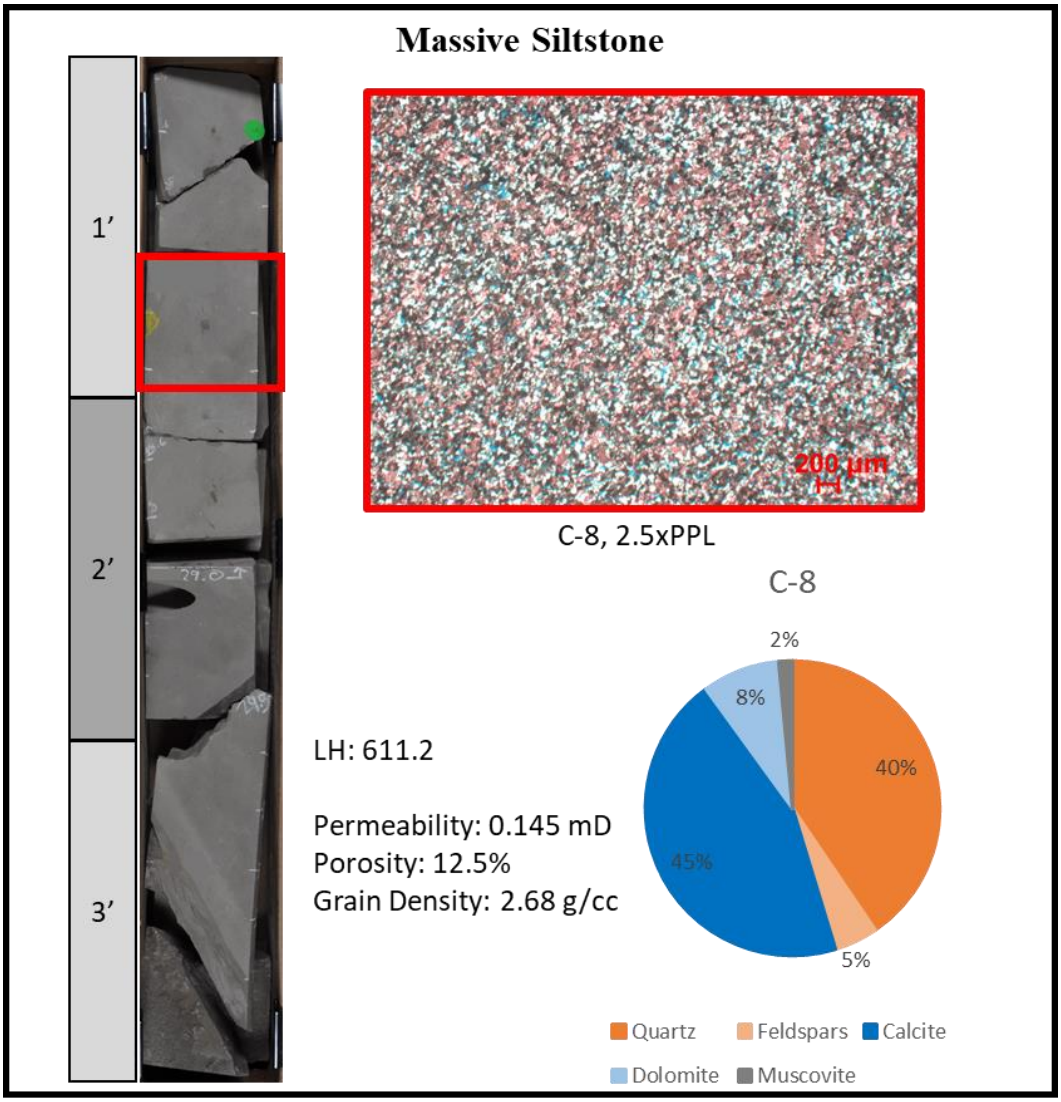

Figure 11: Massive siltstone lithofacies in core, thin section, XRD bulk mineralogical composition, and reservoir properties. The lithofacies were observed in core first and then in thin section and XRD. The red square represents the location of the thin section and the electric log depth is labeled above. The laboratory results of this lithofacies reveal a higher amount of calcite and dolomite than were observable in core. This sample has the one of the highest porosities of the 17 tested samples and a high permeability as well. The core exhibits several bedding angles due to discontinuous slabbing.

4.1.5. Laminated Siltstone

The laminated siltstone facies is present in the lower Sycamore transition zone, lower silty section, and middle Sycamore silty section. The unit exhibits laminations, has no

bioturbation (BI: <1), and appears in lighter to darker shades of grey in core. It is represented by thin section C-13 (figure 12) and contains 38.3% tectosilicates, 57.7% carbonate minerals, 3.1% phyllosilicate mineralogy, and 0.9% additional minerals. This section carries vertical fractures which seems to be associated with higher calcite content. This will be discussed in greater detail in Section 4.1.8.

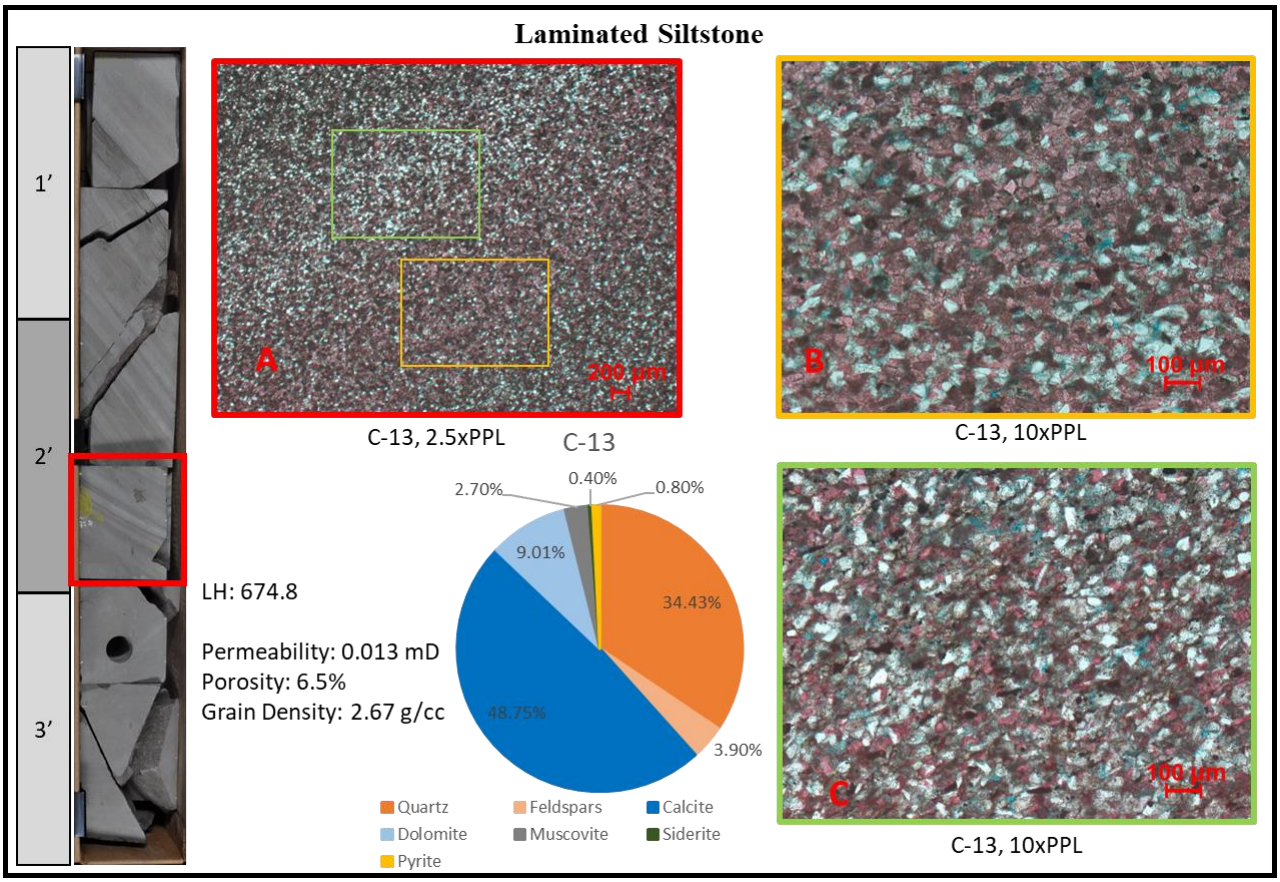

Figure 12: Sample C-13 taken from the laminated siltstone section of core (left) with corresponding results. Laminations visible in core are represented in thin section (photomicrograph A). The red alizarin stain shows where the calcite is concentrated as opposed to where silt grains are concentrated. Upon closer review (photomicrographs B and C) the calcite becomes more apparent as a cement present in B and not as present in C. Porosity and permeability values are medium to low compared to other siltstone lithofacies.

4.1.6. Bioturbated Siltstone

The bioturbated siltstone lithofacies appears to have no sedimentary structure but does have burrows and is commonly overlain by a laminated and/or burrowed thin layer of mud at the top of each interval. Massive siltstones commonly grade up into bioturbated siltstones where the mud layers are present. Bioturbated siltstones appear massive and have burrows, usually subtle in appearance (BI: >1). This lithofacies was further observed petrographically in two thin sections, C-7 and C-9 (figure 13).

The core looks similar where these two samples were taken, but during petrographic work and further review of the XRD results a significant difference was noticed between the two. The first sample C-7 has a higher carbonate content which is apparent in thin section and in the XRD results. Dolomite accounts for 20.5%, with calcite 39.2%, 33.4% quartz, and 3% feldspar. The sample has a porosity of 8.3% with a density of 2.71 g/cc. The second sample C-9 has less calcite cement than C-7, and has similar character of angular silt grains. The lesser calcite composition is likely because the sample has less calcite cement and possess moldic porosity. The porosity is 14.7% in C-9 and grain density is 2.65 g/cc, which is less dense than the cemented C-7 sample. Both samples contain allochem constituents such as echinoderm and bryozoan fragments of varying sizes which exhibit varying degrees of remineralization.

The varying amounts of calcite and dolomite between the two sections is an example of various degrees of cementation within the same lithofacies. This is important to note, although hand samples look similar, differences in diagenetic events affected the porosity and permeability of the sections. The section represented by C-9 seems to be more favorable to host fluids due to higher porosity and could, if charged, be more likely a candidate to be a reservoir

rock. However, the section containing more calcite in C-7 may likely be more favorable in terms of frackability. In core, sections with a higher calcite content often exhibits vertical fractures with calcite cement.

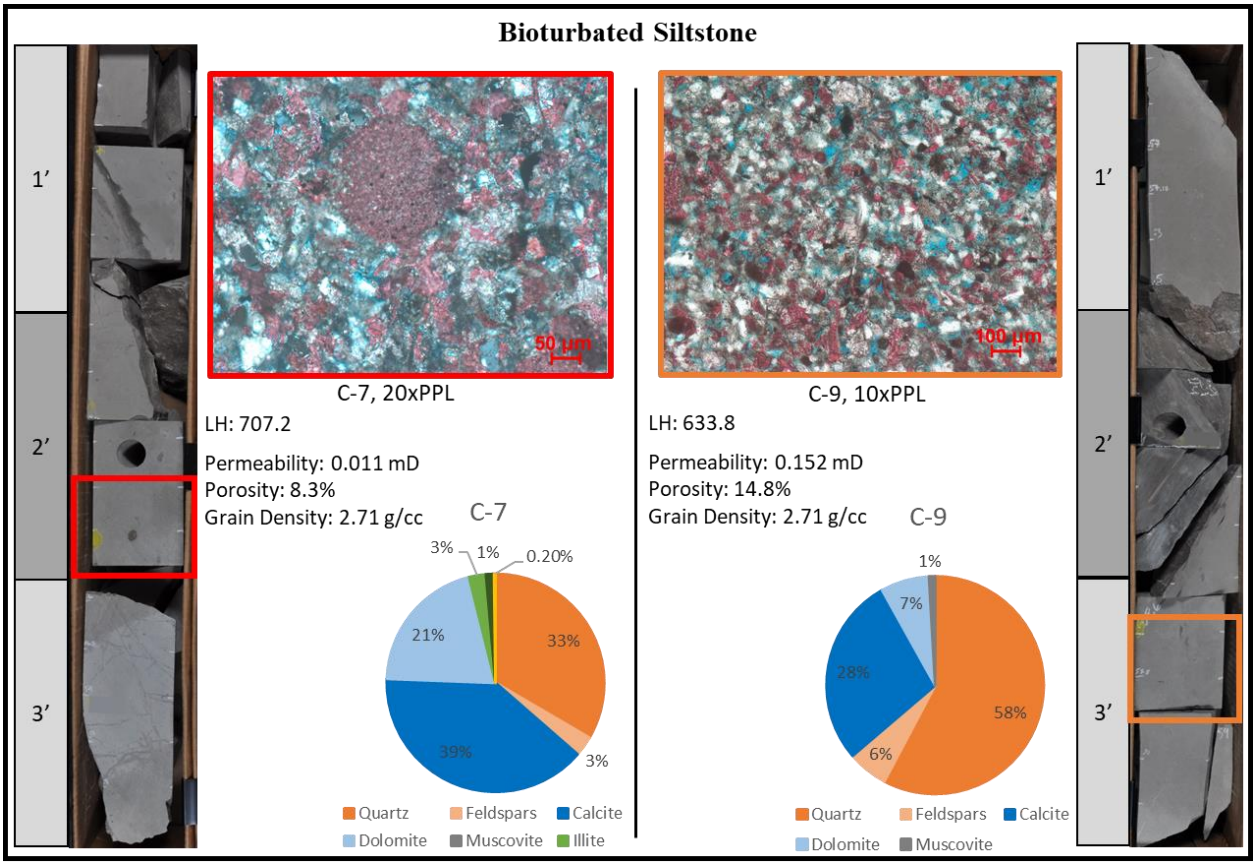

Figure 13: The bioturbated siltstone lithofacies is represented by samples C-7 and C-9. The defining component for this lithofacies in hand sample is a massive appearance with a bioturbation index of greater than or equal to one. The samples exhibit varying degrees of calcite cementation, but the presence of burrows drive their label. Systematic to the features in the core are the overlying muddy sections. Within thin section the C-7 sample shows calcite cement and biogenic grains (echinoid) along with the angular silt grains. In Sample C-9 higher porosity is visible (blue spaces) amongst the angular silt grains and minimal calcite cement. The pore spaces appear moldic, implying secondary porosity.

4.1.7. Laminated Bioturbated Siltstone

The laminated bioturbated siltstone lithofacies are identified in core samples as simultaneously containing both classifiers. The laminations within this facies are visible and were overprinted by burrows with a BI of 2 or greater. This facies also appears more argillaceous, as it is a darker gray to brown in core sample.

Six thin sections were identified within this lithofacies; C-2, C-3, C-5, C-6, C-11, and C-16 (figure 14). The grains in thin section appeared oriented along laminations. Laminations and planar burrows exhibit flocculated silt grains and flocculated clay, distinguishing the sorted material. Within the angular quartz dominated burrows, the grain sizes range from coarse (0.063 mm) to fine (0.002 mm) silt with minimal clay material (figure 14). The clay floccules contain over 85% clay and the medium to finer silt grains remain. Calcite cementation is minimal, and some pore space is preserved on the grain floccules. Present within this lithofacies as well are silicified shell fragments, pyrite spherules, and some blocky calcite cement. The mineralogical percentages for quartz range 30-45%, 7-13.6% feldspars, 0-11.4% calcite, 7.4-23.4% dolomite, 24.6-34% clay, and 1-3.4% pyrite. The samples considered in this lithofacies probably have the greatest range in mineralogical composition because of the broad classifiers.

Sequences of the laminated bioturbated lithofacies were likely deposited under quieter conditions, implied by the very presence of vertical bioturbated silt. The laminations speak to a quieter or more consistent flow regime that supported the system with mixed materials. The increased amount of clay material may imply more distal disposition along with the presence of the Cruziana ichnofacies.

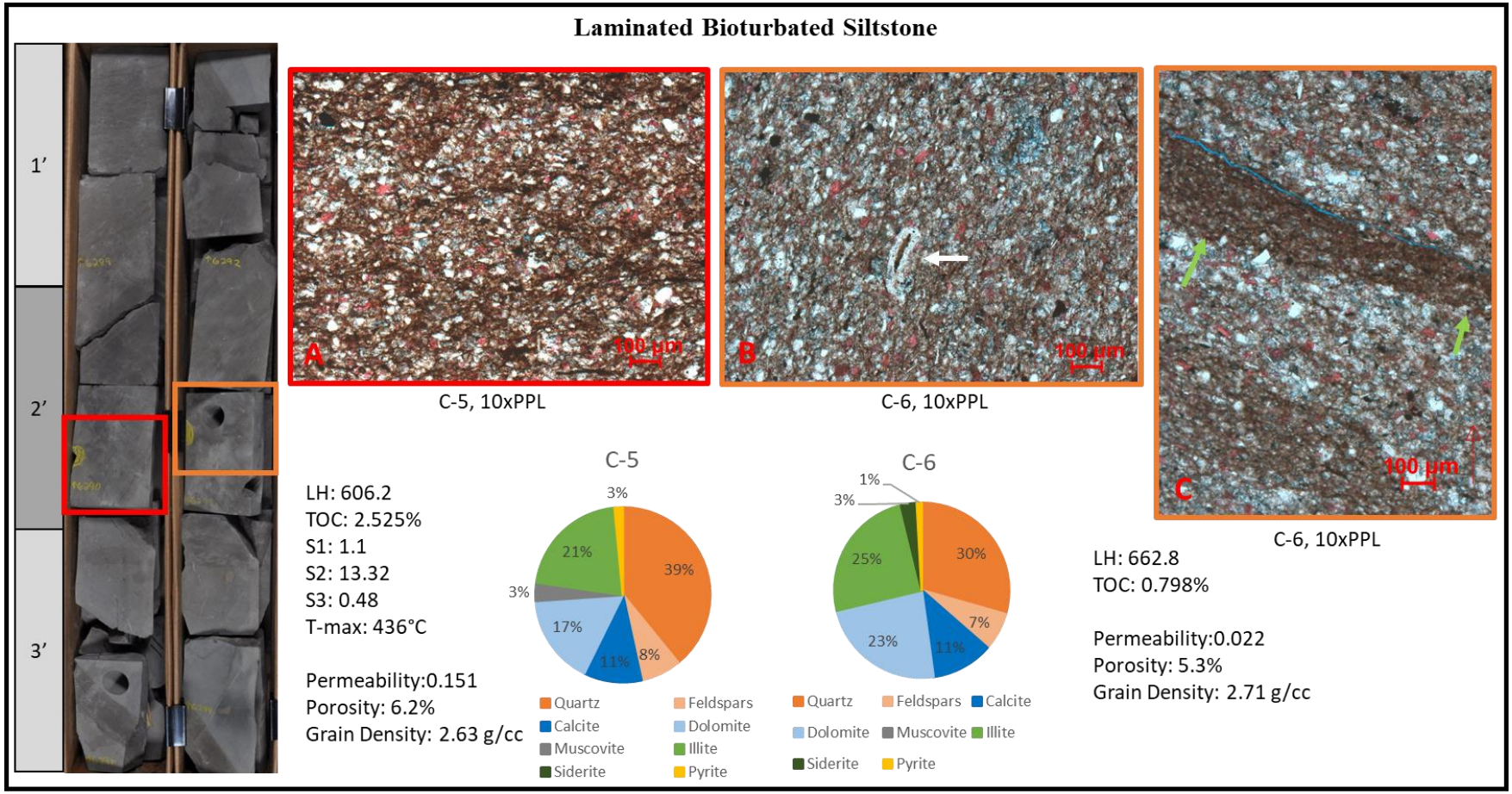

Figure 14: The laminated bioturbated siltstone lithofacies featured in core and thin section, is the most common within the samples taken from the core. The composition is revealed by bulk XRD as having high 35-50% tectosilicate (quartz and feldspar) material, about 30% carbonate (calcite and dolomite) material, and 30% or less phyllosilicate (micas and clays) material. Silt grains can be seen as coarse to fine silt within all three photos. In some areas the silt grains are concentrated amongst argillaceous matrix in photomicrograph A. In photomicrograph C flocculated clay material can be seen (green arrows) and below this concentrated silt grains underlain by more argillaceous material. In photomicrograph B the white arrow points to a collapsed agglutinated foram indicative of a benthic environment.

4.1.8. Massive Calcite Cemented Siltstone

The massive calcite cemented lithofacies is a grey color, structureless in hand sample, not bioturbated (BI = 0), and vigorously effervescent in core. The C-4, C-12, and C-14 thin sections (figure 15) represent this lithofacies. The common characteristics of all three thin sections include angular quartz grains of coarse silt size, some angular to sub-rounded grains of very fine sand size, pelloids, allochem grains, and a matrix that is dominated by calcite cement. One difference about C-4 that was noted was the presence of medium sand sized allochem grains (500-600 microns). The sand sized allochem grains appeared damaged and the grain fabric was somewhat chaotic as opposed to massive to ordered as in C-12 and C-14.

Mineralogically there are two groups of mineral percentages. In C-12 and C-14 the mineralogy is dominated by calcite at 71.5-77.4%. Quartz is present from 17.7-19.4%, feldspars 3.3-3.4%, dolomite 1.4-5.3%, clay minerals <0.2%, and less than 0.4% pyrite. The porosities for these samples range from 2.9-5.8% with densities of 2.68 g/cc and low permeabilities. Sample C-4 contains a lesser amount of calcite at 40.4%, higher quartz 41.9%, feldspars at 5.6% dolomite at 8.5%, clay minerals at 2.6%, and no pyrite. It had a porosity of 8%, similar density of 2.68 g/cc and higher permeability. The presence of higher amounts of dolomite higher porosity and lack of calcite, when compared to C-12 and C-14, allude to the possibility that C-4 was not as thoroughly cemented and/or minerals were leached out providing the moldic porosity within C-4 and the space for later dolomite to crystalize. An idea regarding the process of deposition of C-4 may be a density or gravity flow. This is hypothesized by information previously stated and the poor sorting of the constituents such as the allochem grains of 600 microns oriented

perpendicular to other allochem grains of smaller (300 microns) size amongst a chaotic matrix (figure 15).

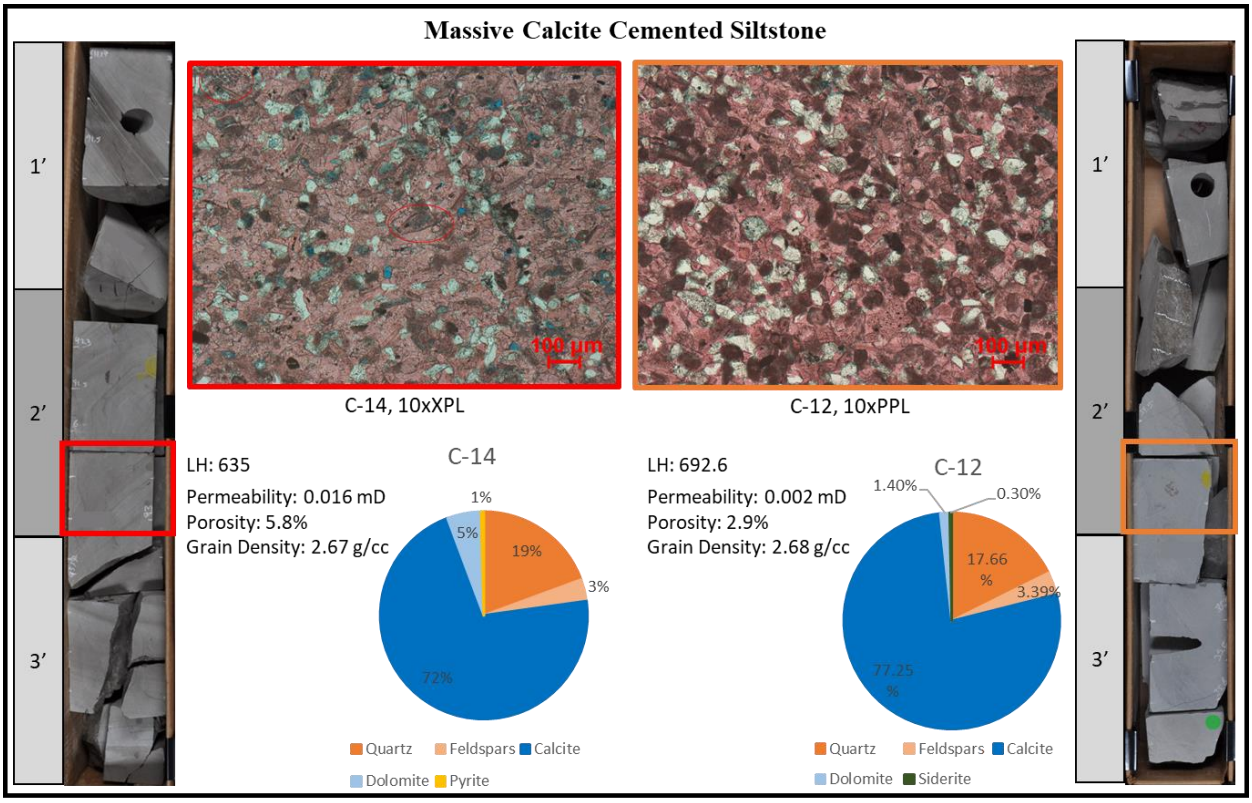

Figure 15: The massive calcite cemented siltstone lithofacies is distinguished in core as having a light gray-blueish color that reveals heavy calcite cement in thin section. Siliciclastic grains are angular to sub-angular amongst carbonate grains (allochems) of shell fragments, bryozoans, fusulinids, and pelloids. Little dolomite and virtually no argillaceous material are present in this lithofacies. Rock property tests reveal low porosity and permeability. Fractures are common in this lithofacies and a vertical calcite filled fracture can be seen in above the C-12 location.

4.1.9. Bioturbated Calcite Cemented Siltstone

The bioturbated Calcite Cemented Siltstone was identified in core only. The main attributes for this blue-grey colored rock consists of vigorous effervescence mostly massive in appearance except for the burrows present. This lithofacies, similar to the massive calcite cemented siltstone lithofacies, exhibit fractures sub-vertical to the bedding plane (figure 16). In some cases, it also exhibits calcite cemented fractures that are vertical like those found commonly in the previously stated lithofacies. Although one thing unique to the presence of bioturbation is the fact that the fractures commonly stem or are relayed through the burrows. The importance of this note is the possibility of fracture propagation in a vertical manner through vertical to sub horizontal burrows. The depositional interpretation of these units is that they were deposited in a setting stable enough to allow burrowing organisms to inhabit the zones. They possess similar amounts of carbonate materials as the massive calcite cemented siltstones that were re-mineralized during diagenesis.

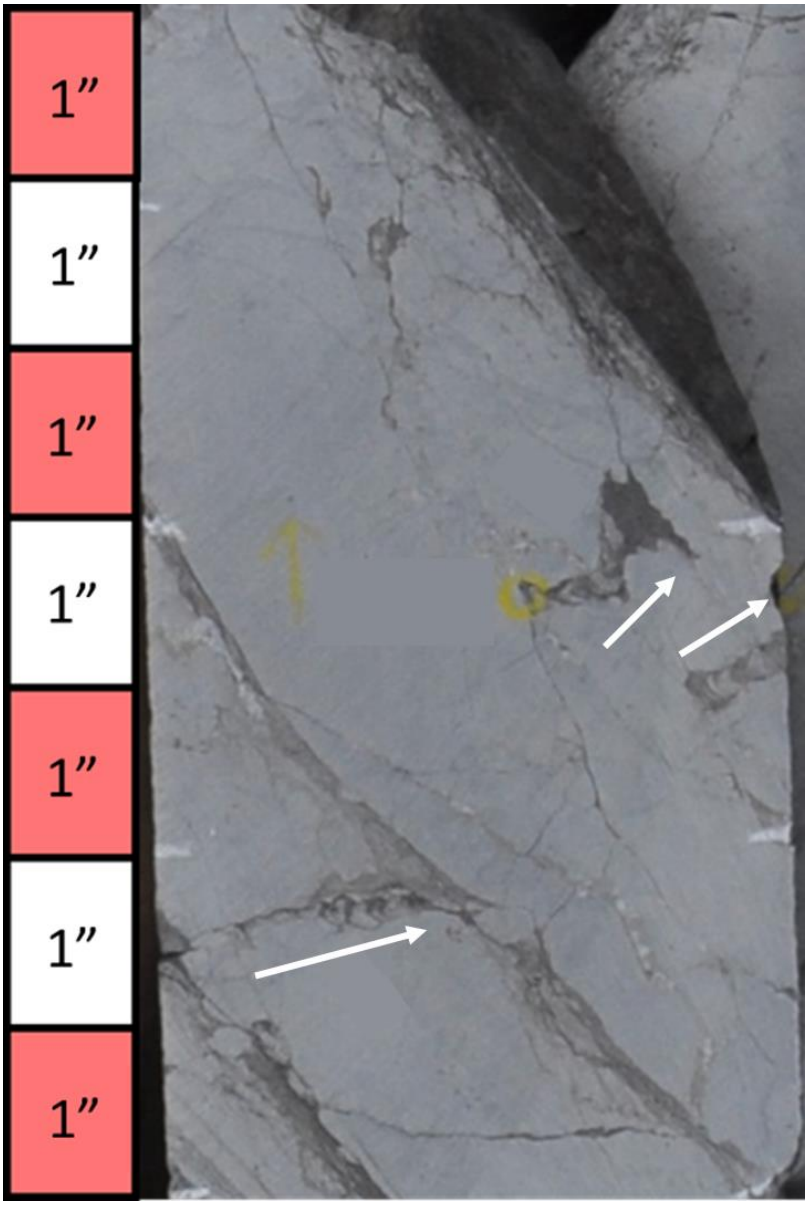

Figure 16: The bioturbated calcite cemented siltstone (BCcSt) appears with a bioturbation index of > 1. The white arrows parallel the burrows and point to the upward direction. Also, fractures propagate through the burrows which are abundant in this lithofacies and in the MCcSt lithofacies.

4.1.10. Interbedded Siltstone

The interbedded siltstone lithofacies was applied to sections of the core where laminated siltstone material and laminated mudstone material were highly alternating. These sections are mixed (figure 17) and they were only identified in core, as a sample was not taken in these intervals.

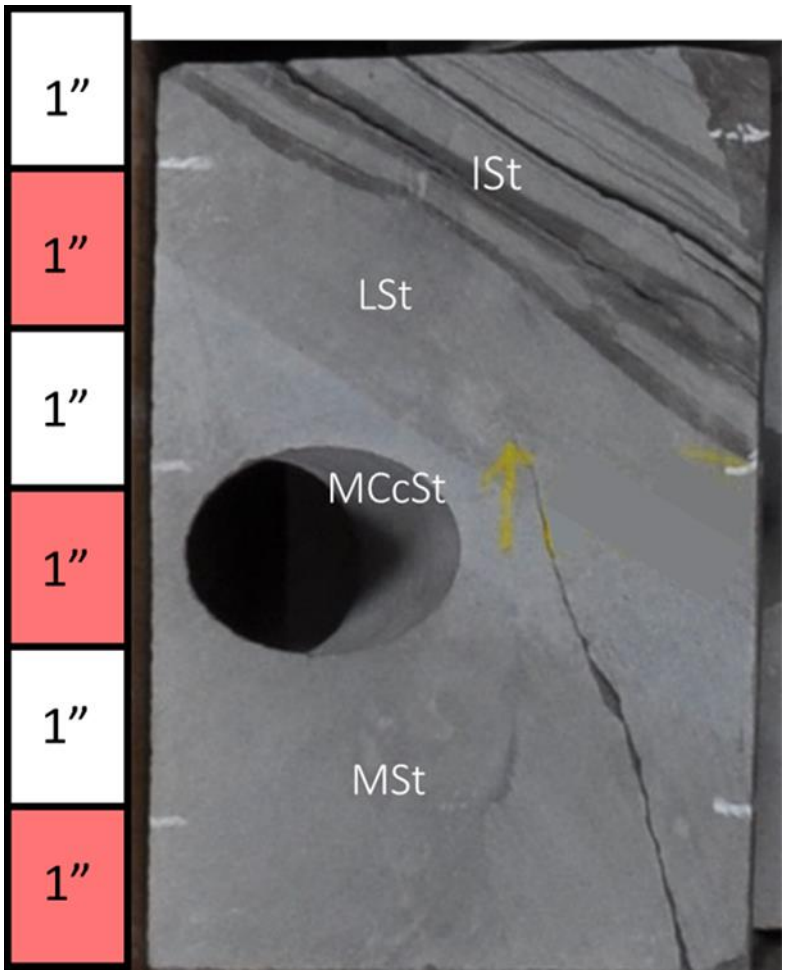

Figure 17: The interbedded siltstone (ISt) lithofacies is a series of siltstone to laminated mudstones. These are found at the top of sequence boundaries and represent periods of alternating sediment supplies.

R/E	Thin Section	Tectosilicates			Carbonates			Phyllosilicates				Other		Total of groups (%)
		Quartz	Feldspars	Total	Calcite	Dolomite	Total	Muscovite	Illite	Siderite	Total	Pyrite	Total	
1.73	C-1	43.8	12.5	56.3	0	4.1	4.1	9.9	27	0	36.9	2.7	2.7	100
1.25	C-2	43.2	13.6	56.8	0	7.4	7.4	13.4	19	0	32.4	3.4	3.4	100
1.32	C-3	50.9	9.3	60.2	4.5	9.2	13.7	12.1	12.1	0	24.2	2.9	2.9	100
1.76	C-4	41.9	5.6	47.5	40.4	8.5	48.9	0	1.8	0.8	2.6	0	0	100
1.63	C-5	39.1	7.5	46.6	10.7	16.6	27.3	3.4	21.2	0	24.6	1.5	1.5	100
1.59	C-6	29.4	7	36.4	11.4	23.4	34.8	0	24.9	2.9	27.8	1	1	100
1.27	C-7	33.4	3	36.4	39.2	20.5	59.7	0	2.5	1.2	3.7	0.2	0.2	100
1.39	C-8	40.5	4.8	45.3	44.7	8.5	53.2	1.5	0	0	1.5	0	0	100
1.53	C-9	57.8	6	63.8	28.1	7.2	35.3	0.9	0	0	0.9	0	0	100
1.35	C-10	45.5	11.4	56.9	0	0	0	13	28.3	0	41.3	1.8	1.8	100
1.54	C-11	36.6	10	46.6	10.4	15.3	25.7	8.9	16.8	0	25.7	2	2	100
1.48	C-12	17.7	3.3	21	77.4	1.4	78.8	0	0	0.2	0.2	0	0	100
1.35	C-13	34.4	3.9	38.3	48.7	9	57.7	2.7	0	0.4	3.1	0.9	0.9	100
1.57	C-14	19.4	3.4	22.8	71.5	5.3	76.8	0	0	0	0	0.4	0.4	100
1.31	C-15	47.8	6.8	54.6	0	9.8	9.8	13.8	18.3	0	32.1	3.5	3.5	100
1.33	C-16	45.1	7.8	52.9	1.2	8.9	10.1	11.7	22.3	0	34	3	3	100
1.65	C-17	41.9	7	48.9	16.4	8	24.4	24.3	0	0	24.3	2.4	2.4	100

Table 6: XRD results

4.2. Core Observations

The X-1 core exhibits 5 major sections of the Sycamore Formation, (1) the Lower Transition Zone (LSyT), (2) the Lower silty section (LSySt), (3) the Middle Sycamore Shale Section (MSySh), (4) the Middle Sycamore Siltstone Section (MSySt), and (5) the Upper Sycamore shale (USySh) (figure 18). Sections not featured in this core are the lowermost transition zone and the upper Sycamore, although they can be seen and correlated in well logs. Well depths were shifted in this thesis for proprietary purposes. The X-1 was drilled in the 1980s targeting a prospective conventional reservoir within the Sycamore Formation in the Velma field of eastern Stephens County. Unfortunately, the well was dry, devoid of both hydrocarbons and water, to the extent that little water came up during drill stem tests. The well reached total depth

(TD) at 5,700 ft. at the Woodford shale and the kelly bushing (KB) was 8 ft. The core was taken from 5,548-5,270 ft. (5,540-5,262 ft. with KB).

The core taken for the X-1 well represents the upper transitional Sycamore, lower siltstone, middle shale, middle siltstone and most of the upper shale. Sections were determined by tying the gamma ray log to the Fox Alliance #1 well from Coffey (2001), to the outcrop sections observed by Milad 2019, and by using the stratigraphic column from core observation. Unfortunately, the core does not contain the Upper Sycamore nor the Caney Shale, but these were correlated to nearby wells using electric logs.

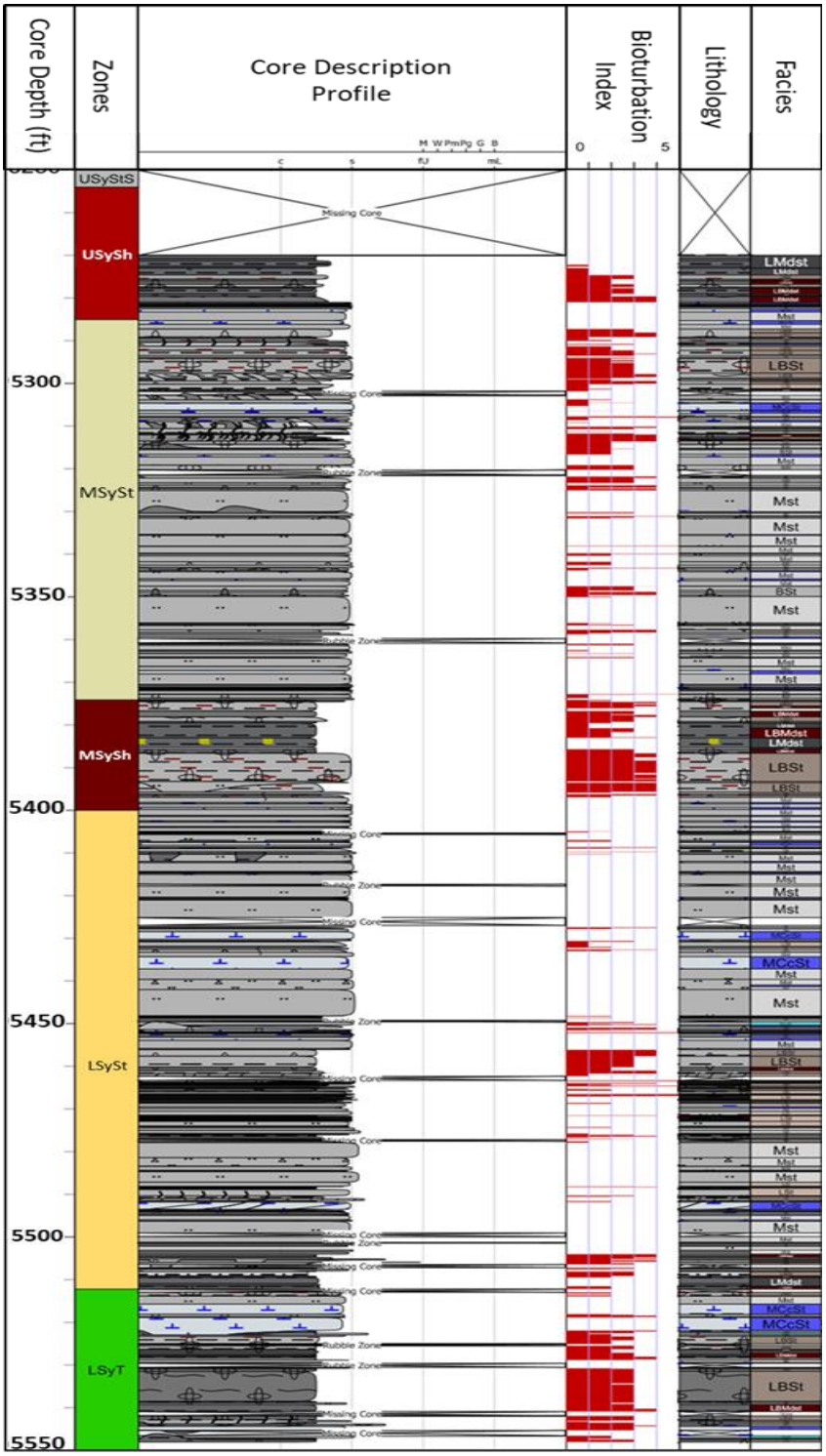

Figure 18: Core log featuring (left to right) sections of the Sycamore Formation, core description profile, bioturbation index, lithology column and Lithofacies ID column. This figure most importantly represents the variability featured within the 5 sections of the Sycamore observed in the X-1 core. Individual (massive siltstone to laminated mudstones) beds are thought to be single gravity flows in the lower siltstone and middle siltstone sections due to the presence of Bouma A, B, D, and /or E in certain intervals.

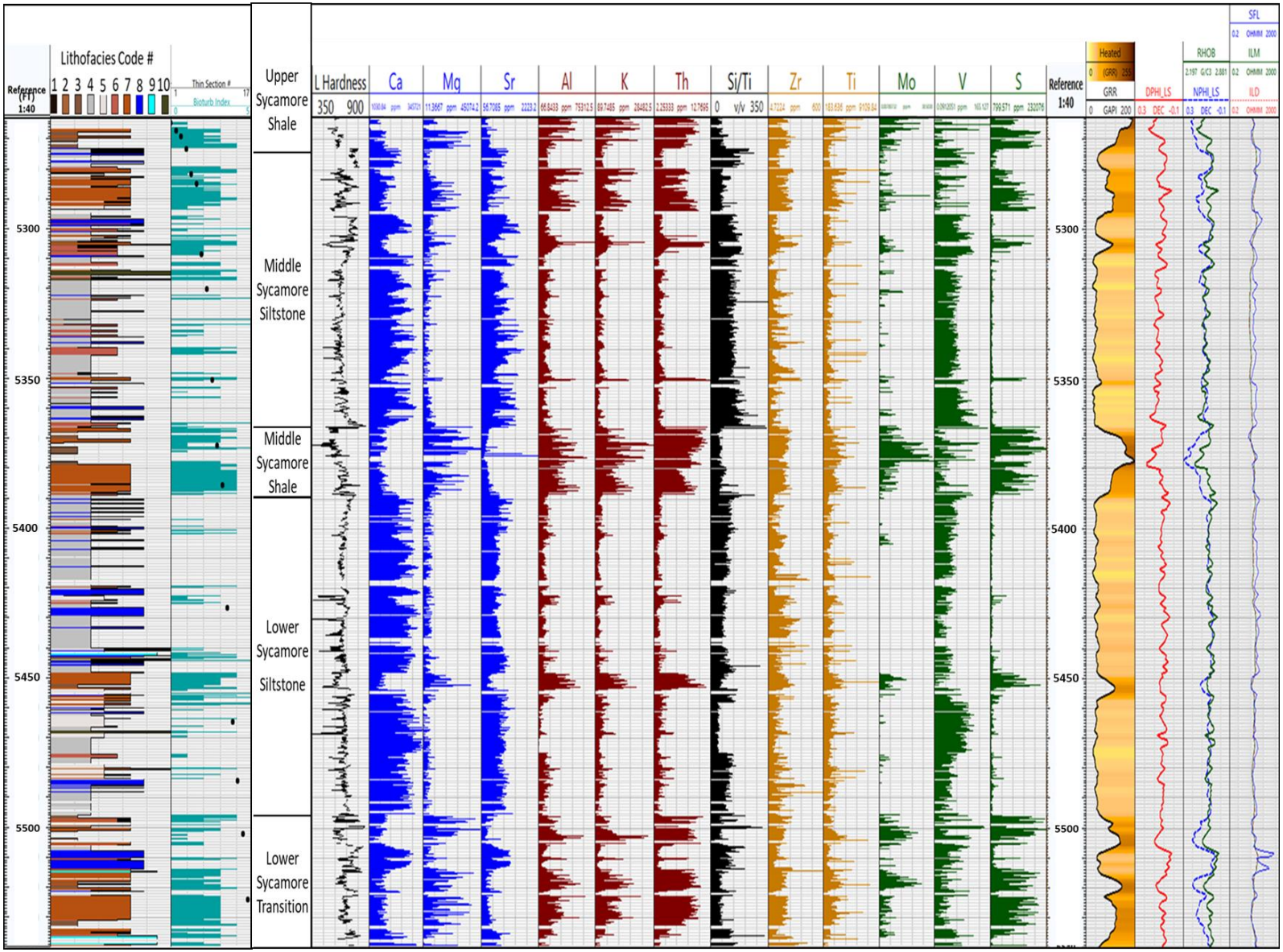

Figure 19: Core lithofacies, Bioturbation Index (BI), XRF results, and well logs.

The Lower transition zone highly varies in lithology. In well logs it is marked by the abrupt decrease in log signature (down to around 30 API) at the base of the Sycamore and top of the Woodford Shale. The upward log signature has an increasing trend (up to 150 API). The top of the Lower Sycamore Transition zone is marked by decreasing API along with an abrupt decrease in porosity and increase in permeability. The lithofacies observed in this section of the core was dominated by the Laminated Bioturbated Siltstone (LBSt) and included the following lithologies as well, LSt, BCcSt, MCcSt, MSt, BSt, and LBMdst. The bioturbation index ranged from a scale of 0 to 5, zero being void of bioturbation and five being completely overprinted by bioturbation. This section accounted for 34 ft. (5,540-5,506 ft. WL depth) within the core but only represents the uppermost extent of the Lower Sycamore Transitional Section.

The Lower Sycamore Siltstone Section consists of more siltstone-based sections that have several lithologic variations and different sedimentary features such as laminations, varying degrees of bioturbation, both, allochem grains, etc. This section has a blocky gamma ray log signature in electric logs with a lower API. It is dominantly the Massive Siltstone lithofacies but also features Laminated Bioturbated Siltstone, Laminated Siltstone, Bioturbated Siltstone, Massive Calcite Cemented Siltstone, Interbedded Siltstones, and Bioturbated Calcite Cemented Siltstone. Towards the middle of this section the facies changes to a Laminated Bioturbated Siltstone (LBSt) for about 10 ft. and appears in the well log as a section of higher API. Above this there are more massive siltstone intervals with fine mud veneers (LMdst) that commonly exhibit burrows (LBMdst). Within several of the Massive Siltstone sections there are allochem grain constituents (crinoid and shell fragments) observed within Massive Siltstone (MSt) sections. The interval makes up 115 ft. of the core.

The Middle Sycamore Shaley Section consists of several sections of laminated bioturbated siltstone that transitions into mudstones. This section is 25 ft. thick beginning at 5,400 ft. core depth (CD) (5,392 ft. drillers depth (DD)) up to 5,374 CD (5,366 ft. DD). The section begins with Laminated Bioturbated siltstones (LBSt) with semi preserved laminations and high degrees of bioturbation (3-4 bioturbation index) which partially to almost fully overprint the laminated fabric of the rock. The section climbs to about 90 API in the LBSt section and spikes to a peak of 200 API in GR response in the upper half of the section. In this zone there is also a lithofacies change to alternating Laminated Mudstones (LMdst) and Laminated Bioturbated Mudstones (LBMdst). In the peak zone (5,386 ft. CD; 5,378 ft. DD) the Laminated Mudstone (LMdst) facies exhibits blocky pyrite within the rock and acicular pyrite around nodules. Within the rest of the section (5,374-5,386 ft. CD) the unit exhibits oval and eye shaped nodules of several inches in size within the mudstone sections, then transitions into the Laminated Bioturbated Siltstone (LBSt) facies and finally into the Middle Sycamore Silty Section.

The Middle Sycamore Silty Section consists of silt dominated lithofacies. In gamma ray log the section exhibits a lowered blocky signature with an average API of 40. This lowered signature can be attributed to the dominant lithofacies; Massive Siltstones (MSt), Bioturbated Siltstones (BSt), and Massive Calcareous Siltstones (MCcSt). Within the top 17 ft. (5,285-5,302 ft. CD) of the section the rock becomes dominantly Laminated Bioturbated Siltstones LBSt) with a bioturbation index average of 3. Within this upper portion of the Middle Sycamore Silty Section the unit is topped by Massive Siltstones and Massive Calcite Cemented Siltstones (MCcSt).

The Upper Sycamore Shaley Section is the last section featured in the core. It occupies the remaining 14 ft. of core (5,284-5,270 ft. CD) and is dominated by the mudstone lithofacies group. The prominent lithofacies being Laminated Bioturbated Mudstones (LBMdst) and Laminated Mudstones (LMdst). Laminated Bioturbated Siltstones are present as well. It should be noted that the core is directly underlying the onset of LBMdst lithofacies, there is a series of alternating Massive Siltstones (MSt) and Massive Calcite Cemented Siltstones (MCcSt).

4.3. Chemostratigraphy Classification

4.3.1. Chemostratigraphy

Chemical signatures visible through the XRF results provided the data to consider chemostratigraphic relationships marked by the presence and/or absence of 13 elemental abundances (figure 20). In the basal section of the Sycamore previously referred to as the transition zone, the elemental abundances vary and host several intervals of clay proxy rich material along with high amounts of S, P, and several smaller Mo rich zones. Concentrations for Ca and Sr are low while Mg varies and is high in the S and P rich zones. In particular the heightened Sr signature may indicate calcite replaced aragonite. The top of this section is identified by a large drop in clay proxy elements, heightened Ca and Sr, and a sudden spike in the Si/Ti ratio below the other changes. A high Si/Ti is thought to be indicative of an increase in non-detrital quartz, and the character of the sudden spike of Si/Ti is thought to represent an algal bloom which deposited biogenic silica.

The second interval is within the section previously referred to as the lower Sycamore siltstone. The characteristics of this section include higher amounts of Ca, Sr, and in the lower half a heightened section of Si/Ti. Al, K, Mo, S, and P are low in this section, indicating a lowered amount of clay input. These observations match the core description.

Within the lower siltstone section an interval of about 10 ft. is dominated by more argillaceous material and exhibits a sudden drop in Ca, Al, and a lower Si/Ti ratio. Inversely the Al, K, and Th elemental abundances spike along with heightened amounts of Mo, S, P, Zr, and Ti. One special component to this interval is the heightened Mg thought to be attributed to higher dolomite.

The upper half of the lower siltstone section is similar to the bottom half except with a sudden spike in Zr and Ti (5,407 ft). The top of the interval ends with a rise in Si/Ti ratio showing another possible location of non-detrital silica present. The Zr ratio remains low at the same depths. The Zr is a valuable proxy because of its association with detrital input. Overall the section appears carbonate proxy dominated with several thinner intervals with input of detrital and non-detrital silica.

The middle Sycamore shale is dominated by heightened Al, K, Th, Mo, S, P, and Mg. Lowered amounts of calcite are present and the Si/Ti ratio is also lower in this section. Corresponding to the highest peak on the gamma ray profile from 5,378-5,370 ft. depth, the Mo peak reaches its highest concentrations. At the top of the middle shale interval is a dramatic change from higher amounts of clay proxy elements, S, and P. the Sulphur and Phosphorous are particularly interesting because they are attributed to anoxic and reducing environments. Within core observation phosphate nodules were observed throughout this interval. A sudden spike in

the Si/Ti ratio marks the boundary of the middle shale and the middle Sycamore siltstone. The presence of a thin Si/Ti interval like this may mark a period of non-deposition at the end of the middle shale section as it also coincides with high S, P, and Mg. All values suddenly drop as the Si/Ti drops at the start of the middle siltstone.

The middle Sycamore siltstone exhibits a serrated pattern across the elements reflecting the cyclicity within, as was described in the core observation results. The section has an overall higher and more continuous Si/Ti ratio than previous sections and the most Mo peaks of the two major siltstone sections. It possesses high Ca and Sr counts although serrated in profile. Mg concentrations are highest in clay proxy rich sections, along with Mo, S, and P. The uppermost part of this section is marked by heightened Al, K, Th, Zr, S, and P with lowered Ca and Sr.

The upper Sycamore shale exhibits heightened clay proxies along with lower Si/Ti ratio and lower Ca and Sr. Mo increases to the uppermost extent of the core along with increasing Al, K, and Th. This interval is highly argillaceous in core and exhibits phosphate nodules with sulfides in hand sample which is reflected in the chemostratigraphic column.

Within chemostratigraphic observations several major themes were noted. Sections with heightened concentrations of Al, K, and Th often exhibit higher Mg which when compared to the XRD and thin section observations can be attributed to the presence of dolomite in argillaceous sections of the Sycamore. Ca and Si/Ti appear to have an inverse relationship. For example, a high count of Ca decreases towards the top of the interval at 5,496-5,474 ft. (WL depth) and the Si/Ti ratio increases.

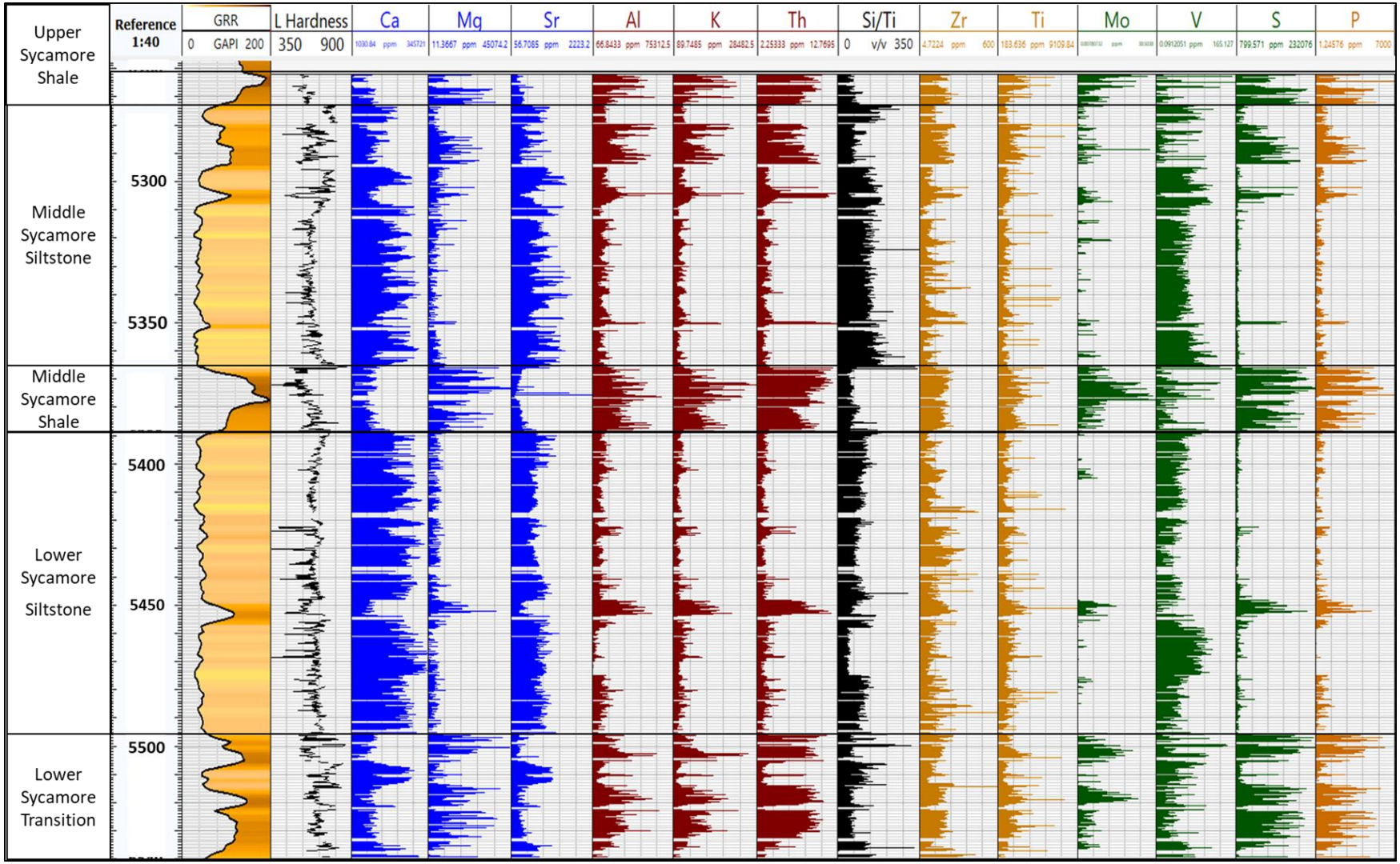

Figure 20: The chemostratigraphic columns labeled by section and compared to the GR log and hardness.

4.3.2. Elemental Compositional Variability

The elemental composition throughout the core was plotted and relationships between elements were compared in relation to lithofacies to observe possible trends. This was done to look at relationships between environmental proxies such as Al and K. These two proxies relate to the clay mineralogies and when high can suggest higher amounts of clay material. Likewise, Ca and Sr are two related elemental proxies that trend positive when carbonate mineral assemblages are present. Relationships between proxies were observed for trends to understand relationships between materials. The main characteristics were positive trends, negative, dual, and no visible trends.

Elements with positive visible trends represent the major mineral groups. Ca, Mg and Sr are major constituents of the carbonate minerals. The trends anticipated should reflect positively between Ca and Sr and Ca and Mg. The first was positive and showed groupings of the lithofacies that were reasonable to observations made in core, petrographic, and XRD analyses (figure 21). The overall trend was positive with a main and branched trend in the measurements with higher values.

Although Ca and Mg are both carbonate mineral proxies the heightened presence of Mg is a proxy associated with dolomite. Ca is present in both calcite and dolomite but where Mg is higher can suggest dolomite. In figure 22 there are two trends. The first is steep and the LBSt, LMdst, BMdst, and LBMdst lithofacies dominate this trend. Then secondly the MSt, MCcSt, BSt, LSt, and BCcSt lithofacies compose a gently climbing trend with much higher Ca ppm counts and low Mg. It reveals that the siltstones have increased amounts of Ca over the mudstone lithofacies and occasional higher amounts of Mg. The one lithofacies that appears to plot

between the two trends is the ISt. This is expected as the lithofacies consists of both muddier and siltier materials as observed in core, thus it respectfully should plot as both.

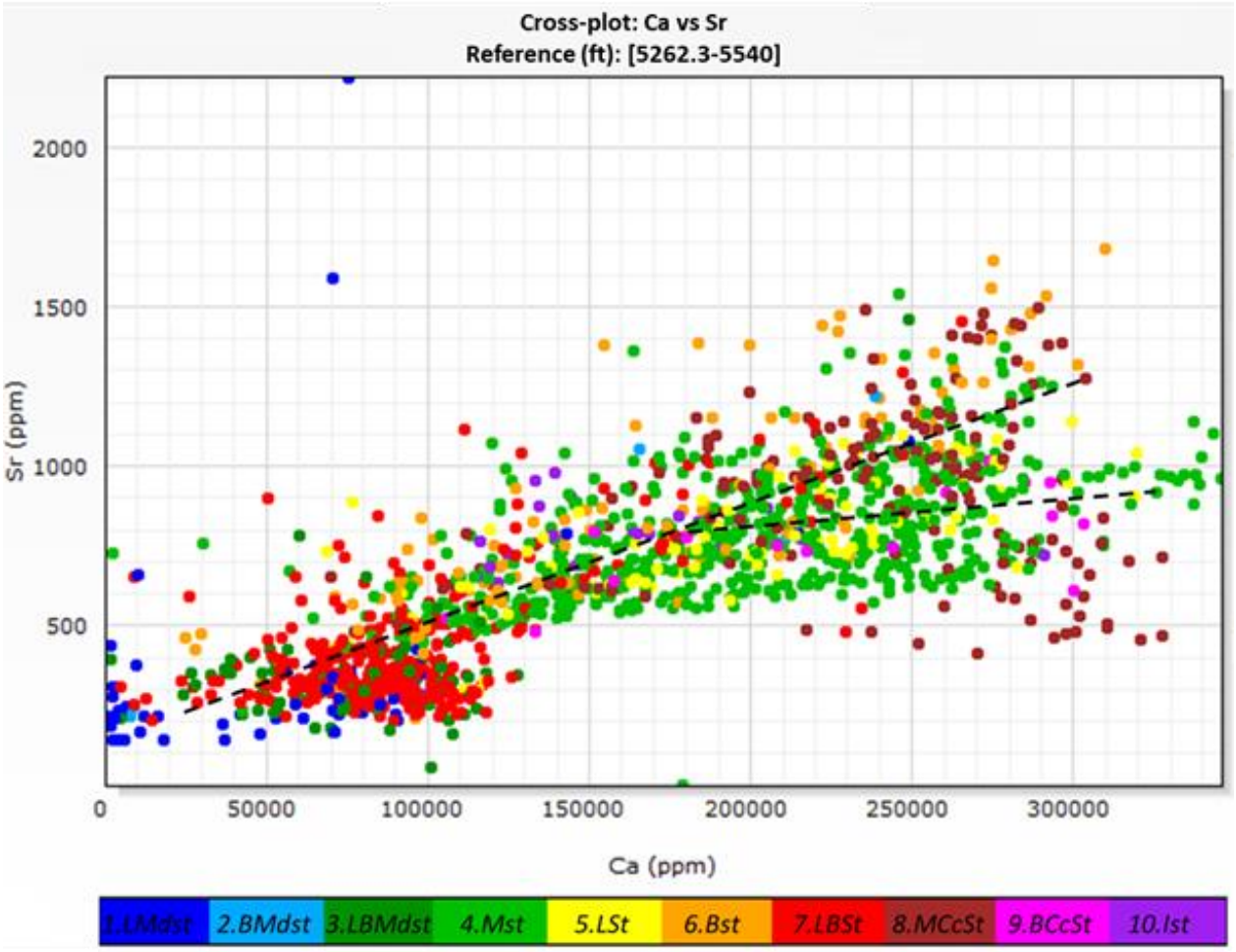

Figure 21: Ca vs Sr cross plot with coloration of the 10 lithofacies. The Carbonate proxies Ca and Sr show a positive trend. Lithofacies which exhibited higher clay content in hand sample, petrographic analyses, and XRD include LBSt, LMdst, BMdst, and LBMdst. These plot low toward the base of the axes with lesser amounts of carbonate proxy elements. The lithofacies MSt, LSt, BSt, MCcSt, BCcSt plot higher counts of Ca and Sr which is matched with observations in other sections of this study. These have more calcite grains and cement.

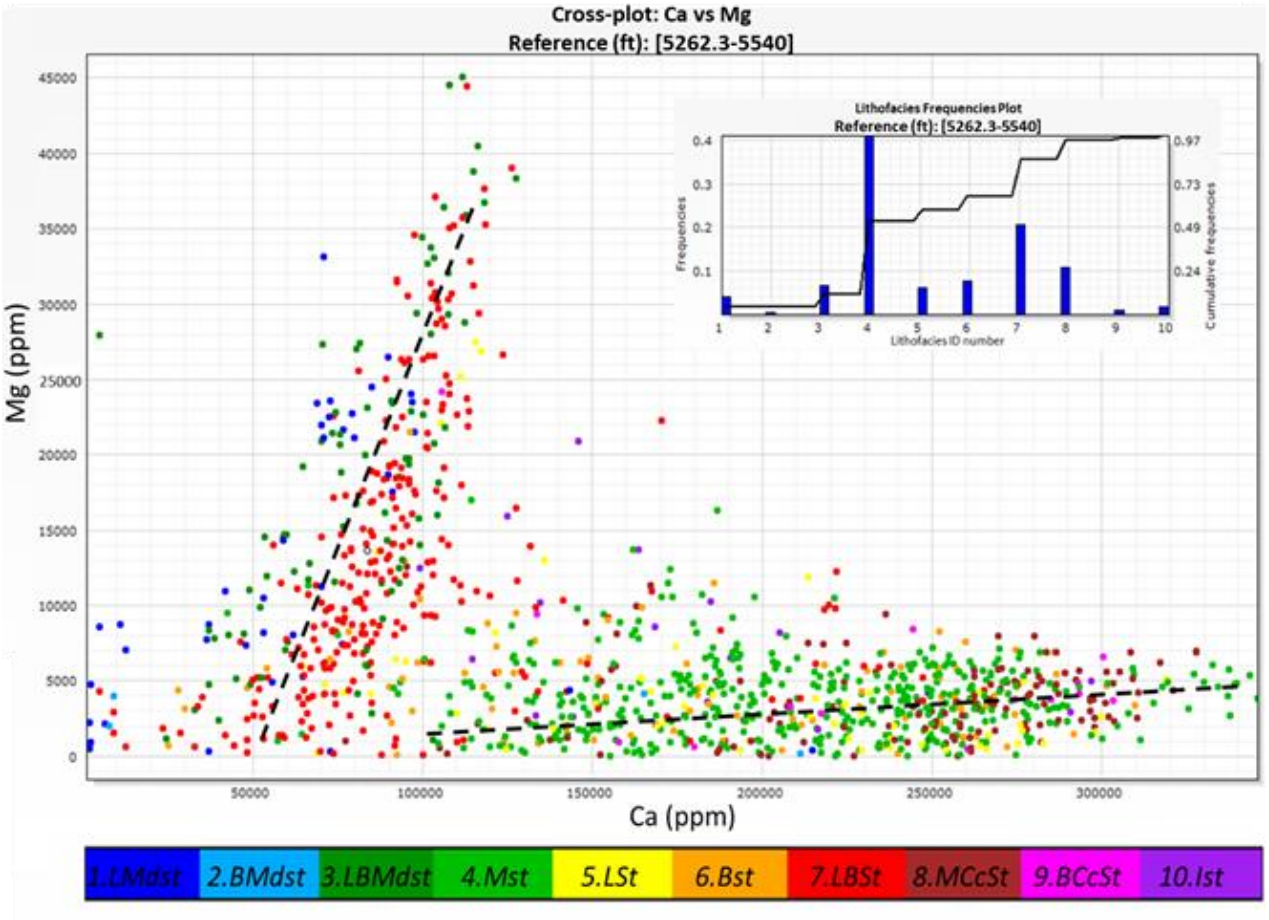

Figure 22: Ca vs Mg cross plot with coloration of the 10 lithofacies. Although the Ca proxy and Mg proxy are both associated with carbonate mineralogies the relationship in this cross plot reveals a higher Mg to lower Ca for the LBSt, LMdst, BMdst, and LBMdst lithofacies. This can be attributed to the presence of dolomite and in general lesser amounts of calcite grains and/or calcite cementation. The second trend shows higher amounts of Ca to overall lower amounts of Mg revealing a higher presence of calcite within the MSt, MCcSt, BSt, LSt, and BCcSt.

Also, positive trending are the Al and K, and Al vs Th plots which serve as clay proxies. Plots for both were observed and showed positive trends. Lithofacies color coding revealed the mudstone grouped lithofacies to plot upwards with the highest values in these plots. High and central to the trend is the LBSt lithofacies underlain by the MSt, LSt and BSt lithofacies. The LBSt lithofacies as previously alluded to and shown in hand sample and thin section contains more argillaceous material while still qualifying as a siltstone by core observation. The siltstone

lithofacies are characterized in this plot as having lower Al, K, and Th counts. The counts become even least for the MCcSt and BCcSt lithofacies. The ISt lithofacies has a separate positive trend in the Al vs K cross plot. This once again is reasonable because the lithofacies is classified by its thin mixed lithologies.

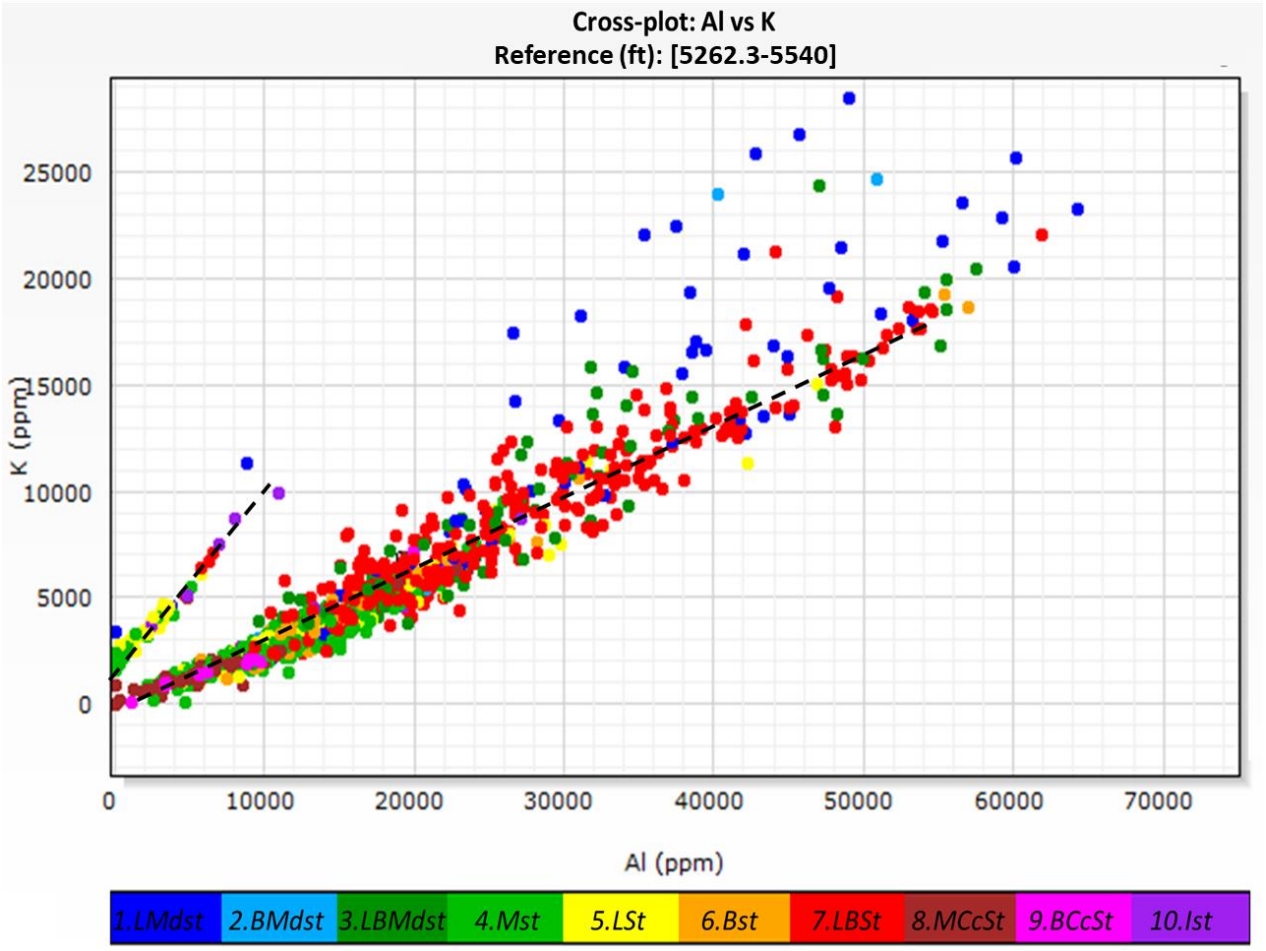

Figure 23: Al vs K plot (ppm) with coloration of the 10 lithofacies. Al and K are proxy elements to clay minerals and in this plot trend positively. The groupings of lithofacies within this plot reveal LMdst, BMdst, and LBMdst as having the highest counts of Al and K. This is followed by the LBSt lithofacies. The MSt, LSt and BSt lithofacies are next and followed by the lowest plotting lithofacies, the calcite cemented siltstones, MCcSt and BCcSt. The ISt lithofacies plots on a separate, steeper positive trend, exhibiting higher amounts of potassium than the MSt and MCcSt.

Negative trending relationships between elements were present in various proxies. Between carbonate and clay proxies (i.e. Ca, Mg, or Sr vs Al, K, or Th) these trends were obvious. For Ca vs K the plot trends steeply negatively with lithofacies LMdst, BMdst, LBMdst, and within the LBSt lithofacies. Lesser amounts of K and Al are observed as decreasing as the Ca concentrations increase (figures 24a & 24b).

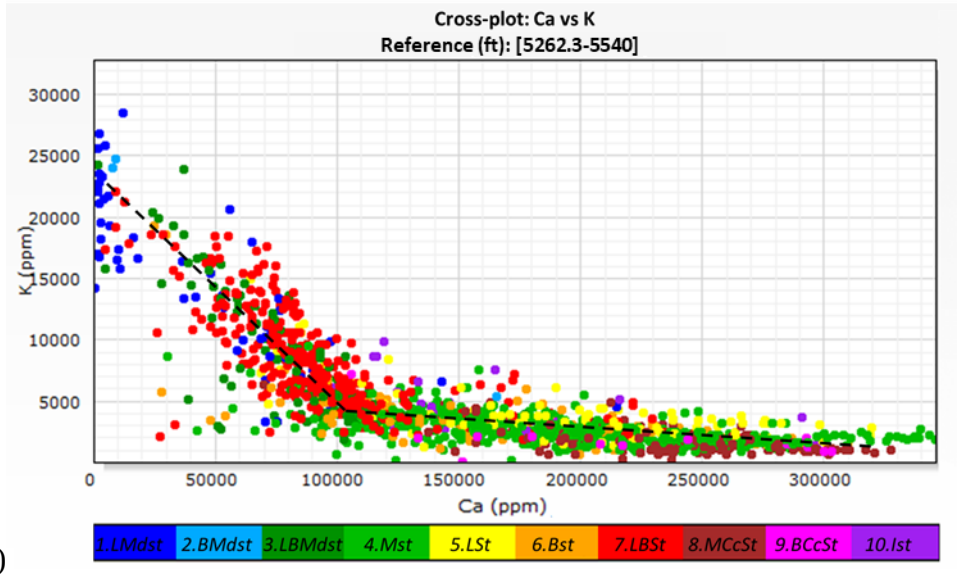

a)

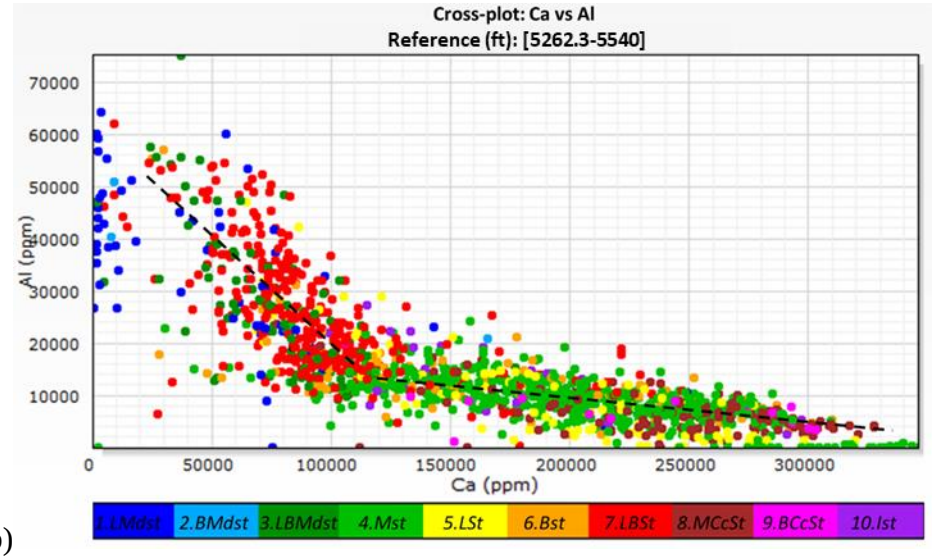

b)

Figure 24: a) Ca vs K and b) Ca vs Al show the negative trending relationships between carbonate and clay proxies. The mudstone based lithofacies and the LBSt lithofacies reveal the heightened amounts of Al and K within these facies.

Negative trends were also observed between Si/Ti vs Zr plot. The mention of this plot specifically is to observe the detrital influence within the units. The muddier lithofacies contained lower Si/Ti concentrations while possessing higher Zr concentrations while siltier and carbonate driven lithofacies were lesser in the amounts of Zr present, except for the BCcSt lithofacies which plotted with the lesser Si/Ti values and higher Zr (figure 25). This particular trend is interpreted to represent a decreasing amount of detrital input, represented by the Zr proxy, as the biogenic silica represented by the Si/Ti proxy increases.

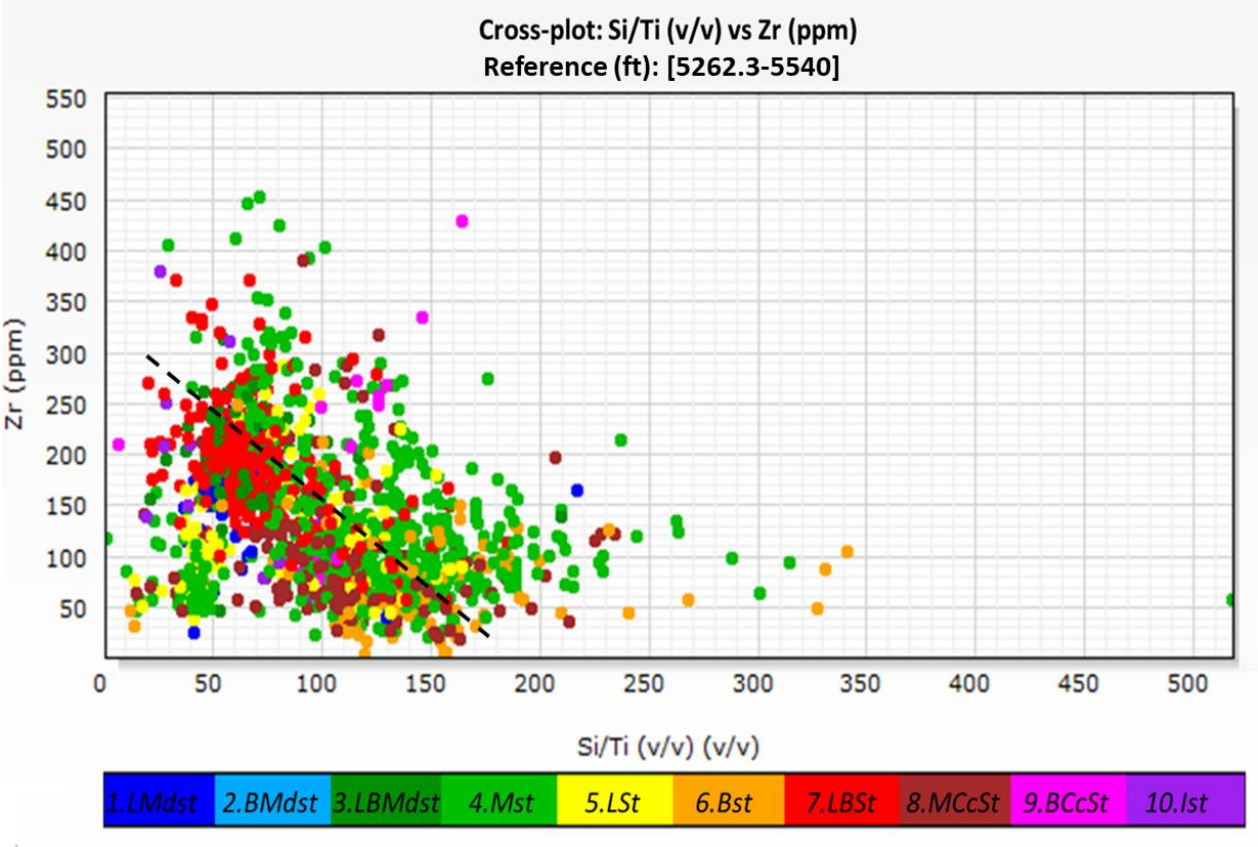

Figure 25: a) Si/Ti (v/v) vs Zr (ppm) shows the negative trending relationships between biogenic silica and allogenic proxies. The mudstones plot low Si/Ti values and higher Zr values. This hypothesized to be related to high detrital input and low biogenic input for the mudstone lithofacies. The MSt, LSt, and BCcSt lithofacies observe medium to high Zr with higher Si/Ti values. This is interpreted to relate to higher detrital input.

Three main groupings were observed through the elemental relationships. Clay, carbonate, and siliciclastic XRF proxies support the presence of these groups. The mudstone lithofacies (LMdst, BMdst, & LBMdst) showed higher elemental abundances that relate to argillaceous materials, with low amounts of carbonate related materials. The siltstone lithofacies (MSt, LSt, BSt, MCcSt, and BCcSt) reveal elemental abundances that reflect two groupings, one higher in siliciclastic material and the other (MCcSt & BCcSt) more carbonate driven. The LBSt and ISt lithofacies plotted between the mudstone and siltstone lithofacies revealing a mix or range within these lithofacies IDs.

4.3.3. Multi-variate Clustering Analysis (MVCA)

Multivariate cluster analysis was conducted using 7 clusters (figure 26). Upon review of the cluster analysis results, chemofacies identified carried various elemental characteristics that distinguished them form one another. A centroid was calculated for each element within the 7 clusters and show the average value for each of the 16 variables. The goal of the MVCA was to quantitatively characterize sections of the core and relate the chemofacies back to the lithofacies identified. The three major groupings thought to be present were hypothesized to reflect mudstones, siliciclastic to mixed and carbonate driven. The following descriptions are the observed differences between identified chemofacies.

The class 1 grouping possesses the highest values of Magnesium with low Ca and Sr. it possesses low Al, low K, and a moderate value of Th. It has the lowest Si/Ti and lowest Si/Al values. It has high values of S and P, the highest Zr and U values along with high Mo and low V. When observing these elemental relationships via the lens of elemental proxies it suggests the

chemofacies represents a dolomitized mudstone facies with high S and P and U. In the lithofacies description process such rock was observed where phosphate nodules were present. The interesting point with this chemofacies is the high Mo values relative to low clay proxy elements (Al, K, and Th), high S, P, and U.

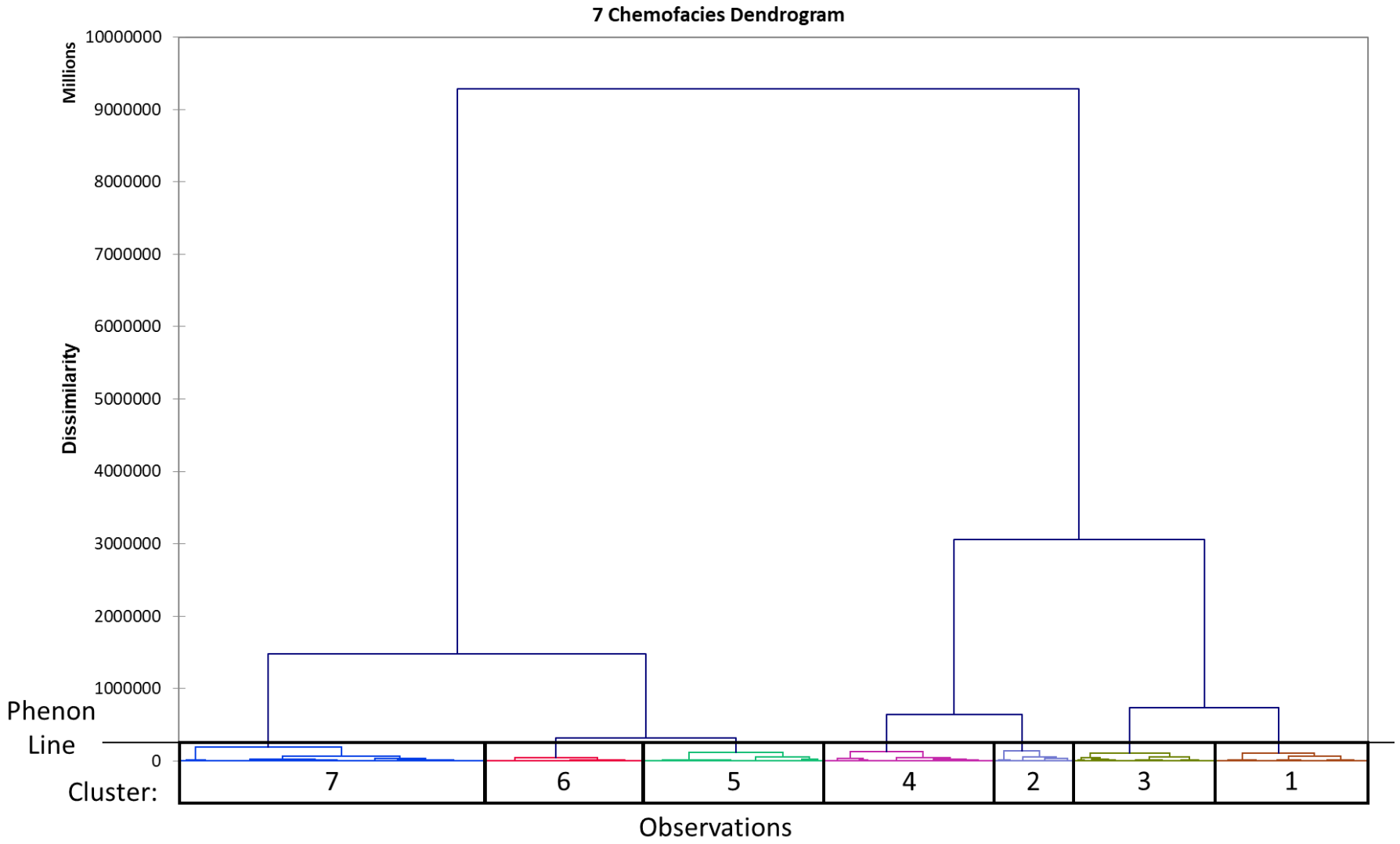

Figure 26: The dendrogram for geochemical data showing the elemental data clustered into 7 groupings. Each cluster represents a chemofacies and possesses unique chemical characteristics. The x-axis represents the number of observations or data points within each cluster. The phenon line is an arbitrary line that marks "the boundary of similarity below which a group will form a cluster" (Turner et al., 2015 after Guler et al. 2002).

The class 2 chemofacies has the highest average values for Al, K, Mo, and V. It possesses high clay proxy values and low values for carbonate mineral proxies. This chemofacies has the highest values for Mo and V. Mo is related to high TOC in the chemostratigraphic section. The class has the least number of objects in the MVCA results. This chemofacies is thought to relate to the mudstone lithofacies.

The class 3 chemofacies has the second lowest and third lowest Ca and Sr values along with the second highest value for Mg. It contains low amounts of carbonate materials and has some dolomite. This chemofacies has the second highest Al and K values with a high amount of Th, representing a high amount of clay material present and a low Si/Ti ratio. The low Si/Ti suggests a higher amount of detrital silica to biogenic material. This is interpreted as correlating to one of the mudstone lithofacies. Present in this class are 171 objects.

The class 4 groupings major characteristic is that it contains medium amounts of the various elemental concentrations except for having the highest value for the Si/Ti ratio. This suggests a mixed composition with a higher presence of biogenic silica. 203 objects are present to this chemofacies.

The class 5 grouping is second highest in Ca, Sr, Si/Al, and second lowest in Al, K, and Th. This suggests a higher carbonate concentration and relatively low amounts of clay material. Concentrations of Mo are negligible, and low S, P, U further suggest an environment of minimal organic material and presence. This class has the second highest number (217 objects) of objects within the population of the whole MVCA analysis.

Class 6 contains high amounts of Ca and Sr with low Mg, representing a presence of high carbonate composition and low dolomite content. The Al, K and Th concentrations are low with

a high Si/Al ratio. The chemofacies class possesses the second highest Si/Ti ratio. This suggests a higher amount of non-detrital silica. It also has low S, P, & U concentrations along with negligible Mo concentrations. This chemofacies is interpreted to be siliciclastic – carbonate mixed with little clay material. The class is represented by 191 objects.

The class 7 chemofacies is the highest in Ca and Sr, lowest in Al, K, Th, Si, Ti, S, P, Zr, Mo, V, and U. This chemofacies has highest concentrations for carbonate materials and minimal concentrations for clay, detrital, and reducing environment materials. Having the highest concentrations for the carbonate elemental proxies and the lowest for clay proxies the class is hypothesized to relate to the calcite cemented lithofacies. Class 7 also contains the greatest number of objects (370 objects). This chemofacies likely upscales several of the lithofacies observed in core.

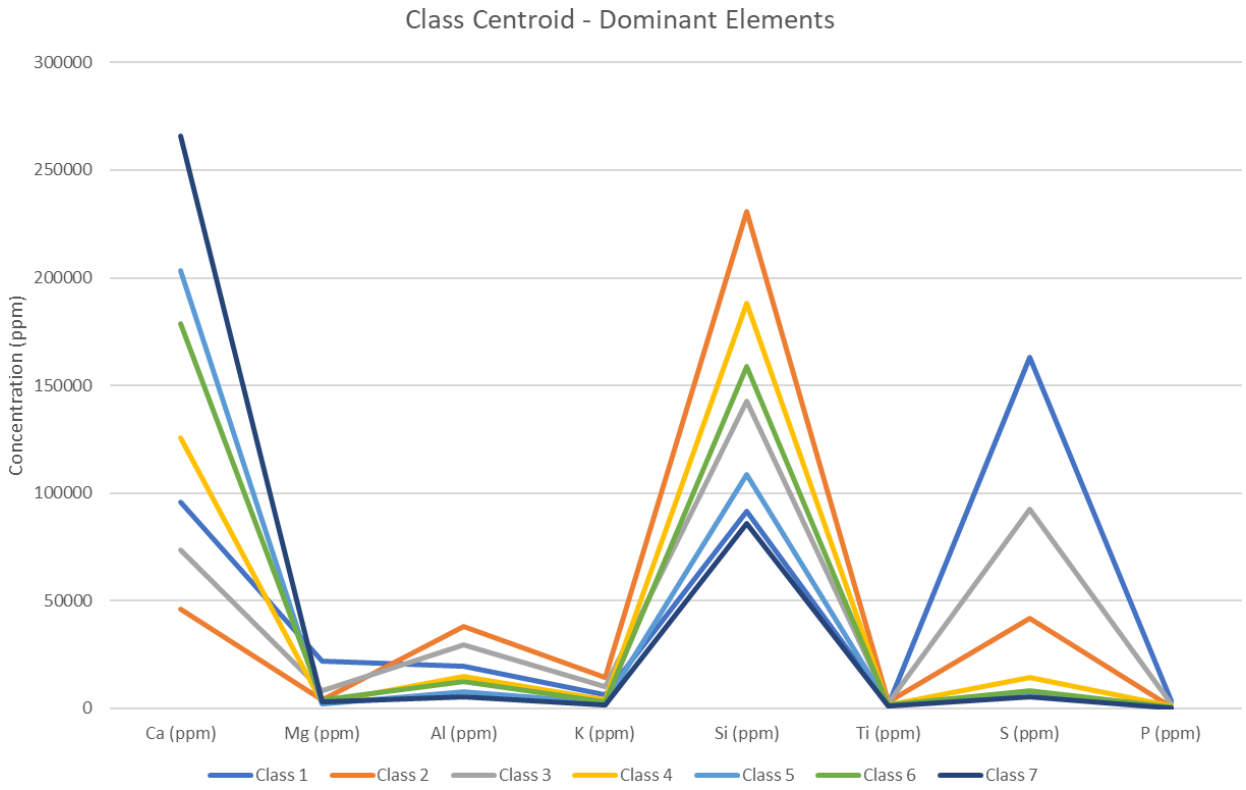

Figure 27: Chemofacies (classes) major elemental abundances.

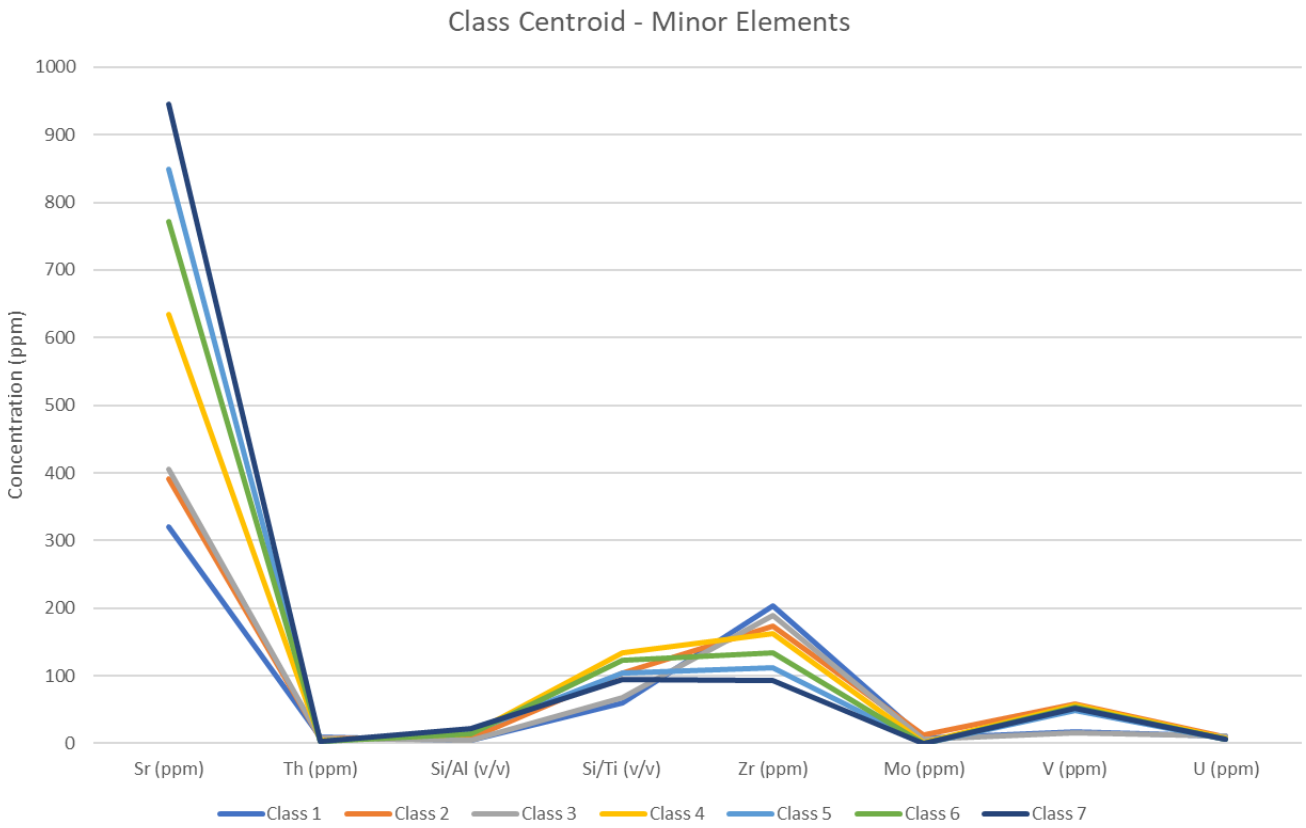

Figure 28: Chemofacies (classes) minor and lesser elemental abundances.

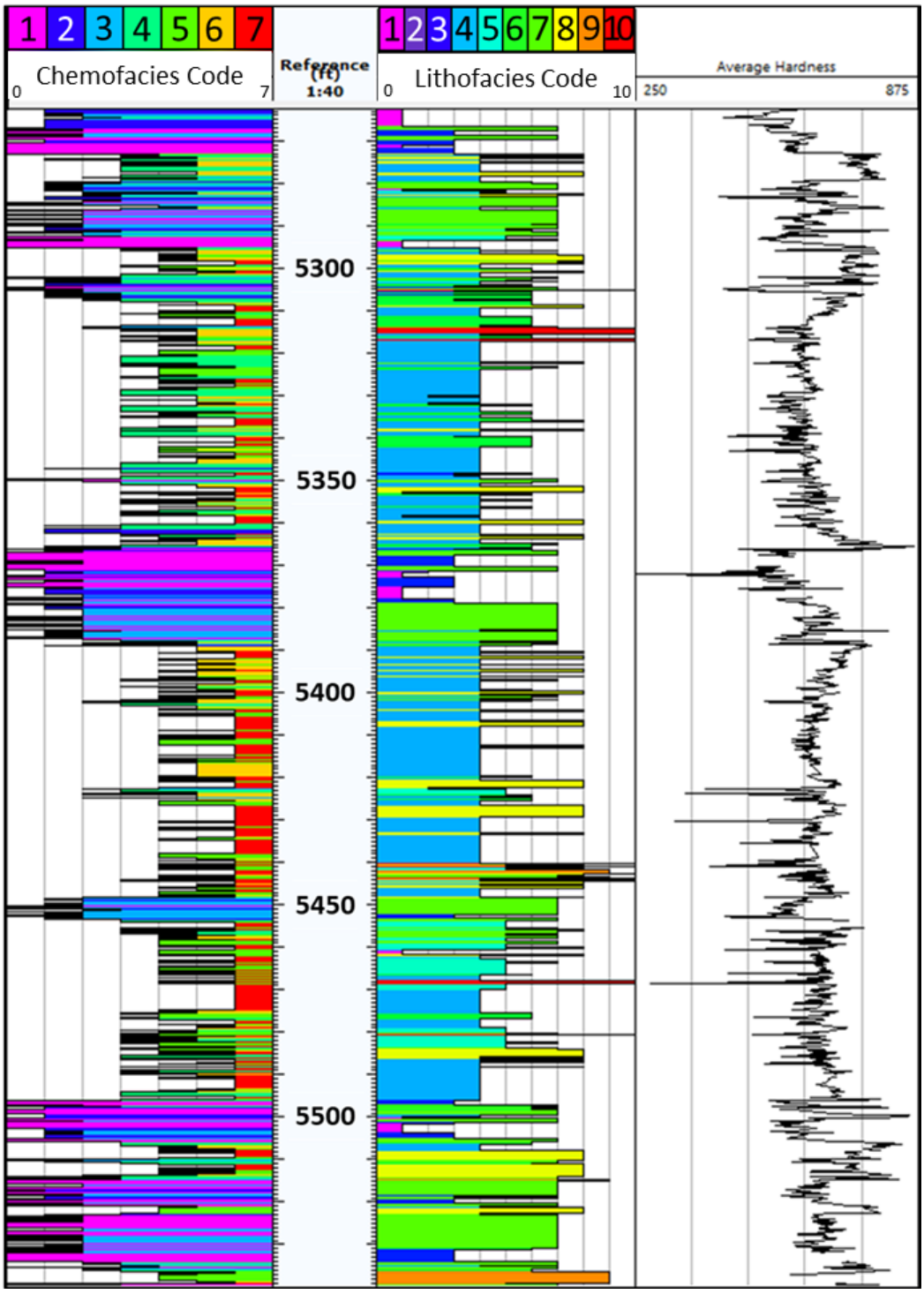

Figure 29: Vertical section of the classes clustered in the MVCA analysis compared to the lithofacies identified in core analysis and average LH. The class color scheme and lithofacies color scheme are not equivalent in value. The primary objective of this figure is to show the detail and chemical variation detected in the chemofacies analysis. In sections like 5,520-5,530 ft. the chemofacies column distinguishes several chemofacies whereas the core analysis distinguishes one main lithofacies.

4.3.4. Rock Eval and TOC Analysis

After rock eval on samples from the shalier intervals of the Sycamore, a more complete picture was painted of the Sycamore shales as internal sources for hydrocarbon generation. The highest Leco TOC measured was 12% and the majority of samples measured between 1.6 to 4.30% TOC. The shallower samples had T-max values less than 435°C, just under the start of hydrocarbon generation. Four of the nine samples possessed a T-max of 435°C and greater. These combined with TOC values ranging from 1.6 to 2.53 have low S1 values and higher S2 values showing the hydrocarbon generation potential is still present within the shaley intervals.

When observing characteristics of the Rock Eval results a trend was observed. Firstly, the presence of organic matter occurred in significant amounts within the shalier intervals. Secondly, the TOC was highest in the shallowest sample and seemed to start out in lesser amounts and increase in the higher GR (API) peaks when matched to the gamma ray log. Thirdly, the deeper samples achieved a T-max sufficient for hydrocarbon generation while the shallower intervals did not achieve this T-max but exhibited good TOC. And fourthly, samples plotted as type two kerogen, matching the environmental observations and exhibiting a decent kerogen quality to hydrocarbon potential (figure 30).

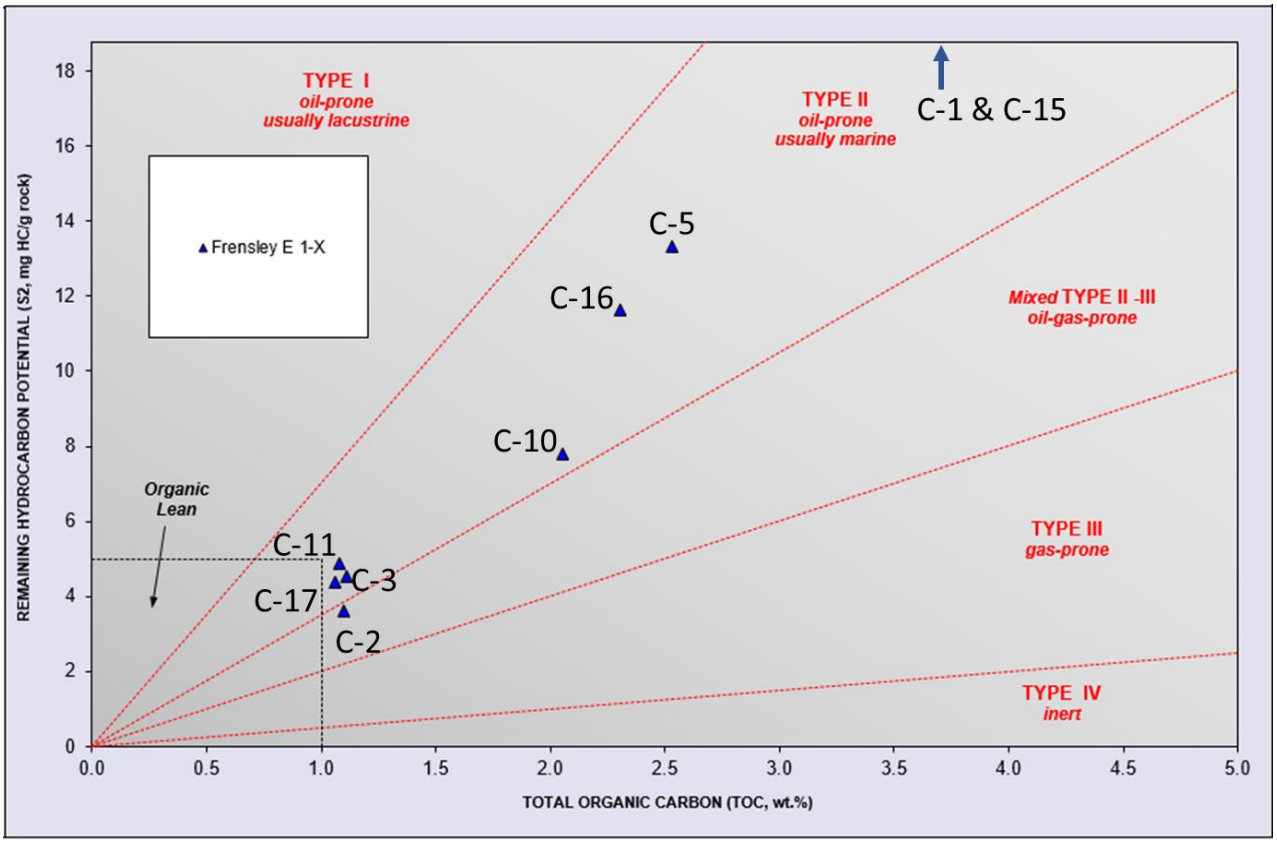

Figure 30: Kerogen Quality plot with samples labeled.

Essentially, the four shalier sequences within the lower to upper Sycamore imply a rise in relative sea level. These intervals provide organic material to the system, but the immature state of the kerogen indicates minimal to no expulsion. The Sycamore within this location is particularly shallow (5,260-5,540 ft.) and organic material is immature within the Velma field as it did not achieve the depth of burial or subsequentially the T-max required for expulsion. The formation achieves greater depth of burial in the nearby Sholem and Tatums fields which may have provided favorable conditions required for oil generation.

4.4. Sequence Stratigraphy

The Sycamore Formation is underlain by the Woodford Shale and overlain by the Caney Shale. Based on gamma ray parasequence (GRP) observations 3rd and 4th order cyclicity was observed. Within the core, sections dominated by siltstone as marked by the black arrows in figure 33 contain an element of cyclicity. The MCcSt lithofacies and the MSt lithofacies transition into the LBSt and ISt lithofacies, followed by the ISt or LSt and are terminated. The terminal boundaries mark the end of a parasequence of 4th or 5th order within the Sycamore.

The GRP observations resulted in 4, 3rd order sequences and numerous 4th and or 5th order GRPs. Figure 33 illustrates these GRPs. GRP 1 trends generally upward in API with many smaller cycles exhibited in the higher order column. The section corresponds to the lower Sycamore transition zone. The upper limit to the section is marked by the last high GR peak. GRP2 begins with the decreased gamma signature and remains relatively low for the section. Internal are two shale intervals, the upper shale marking the top of GRP2. The GPR3 is marked by the low GR signature above the boundary of GPR2. This parasequence exhibits a constant log signature until it begins to fine upwards in the upper half. The upper parasequence boundary is marked by the sudden decrease in log signature. GPR4 is the upper Sycamore siltstone in which the intervals are fairly clean in their log signature. On a 4th order note there is a shaley interval present in the middle of this section but as a 3rd order sequence we observe this sequence up to the boundary of the Caney Shale.

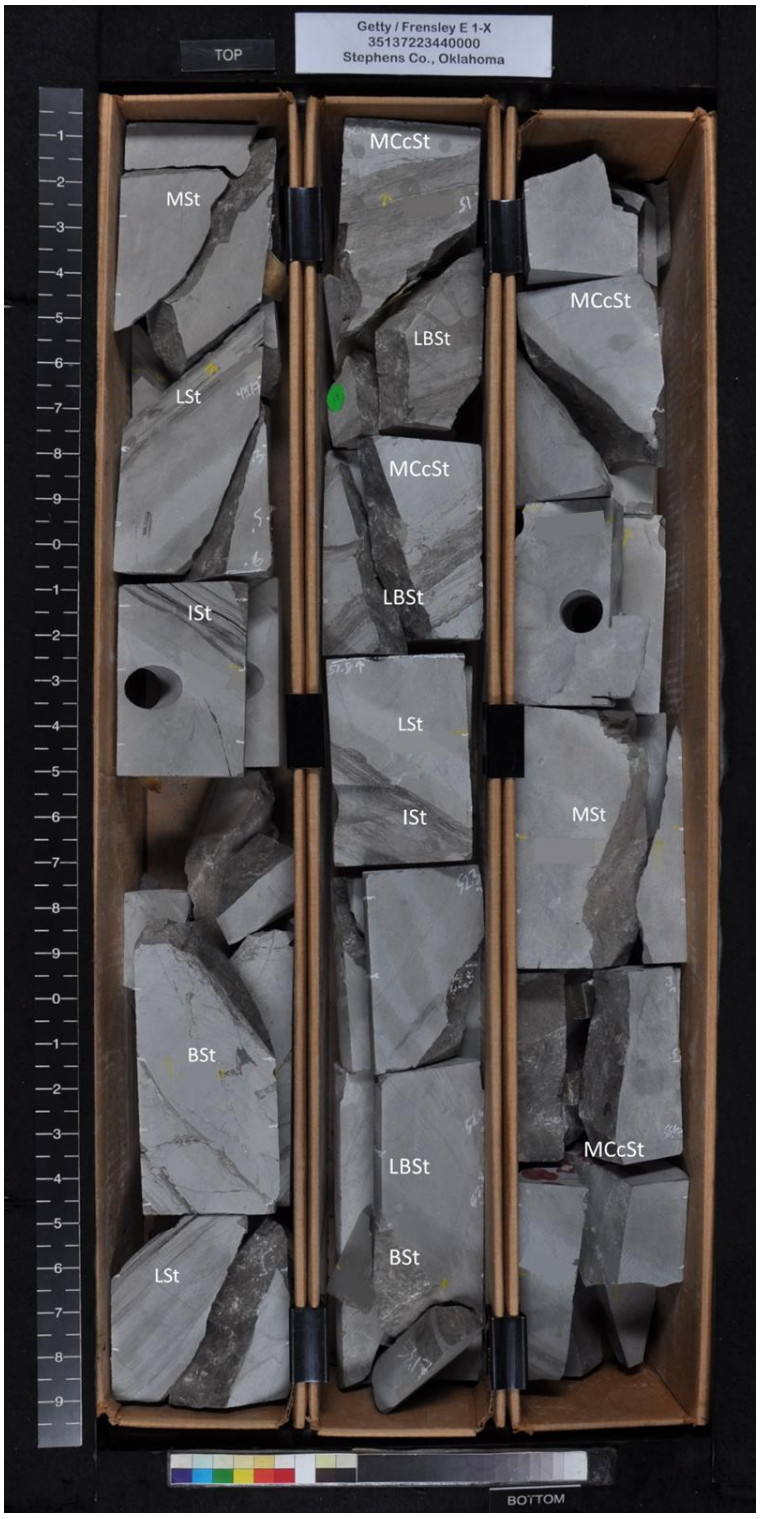

Figure 31: Cycles of the Sycamore within the siltstone sections of the X-1 core. The MSt, MCcSt, and BCcSt lithofacies can be observed as beginning with sharp contacts and grading into the more argilaceous ISt, LBSt and LSt.

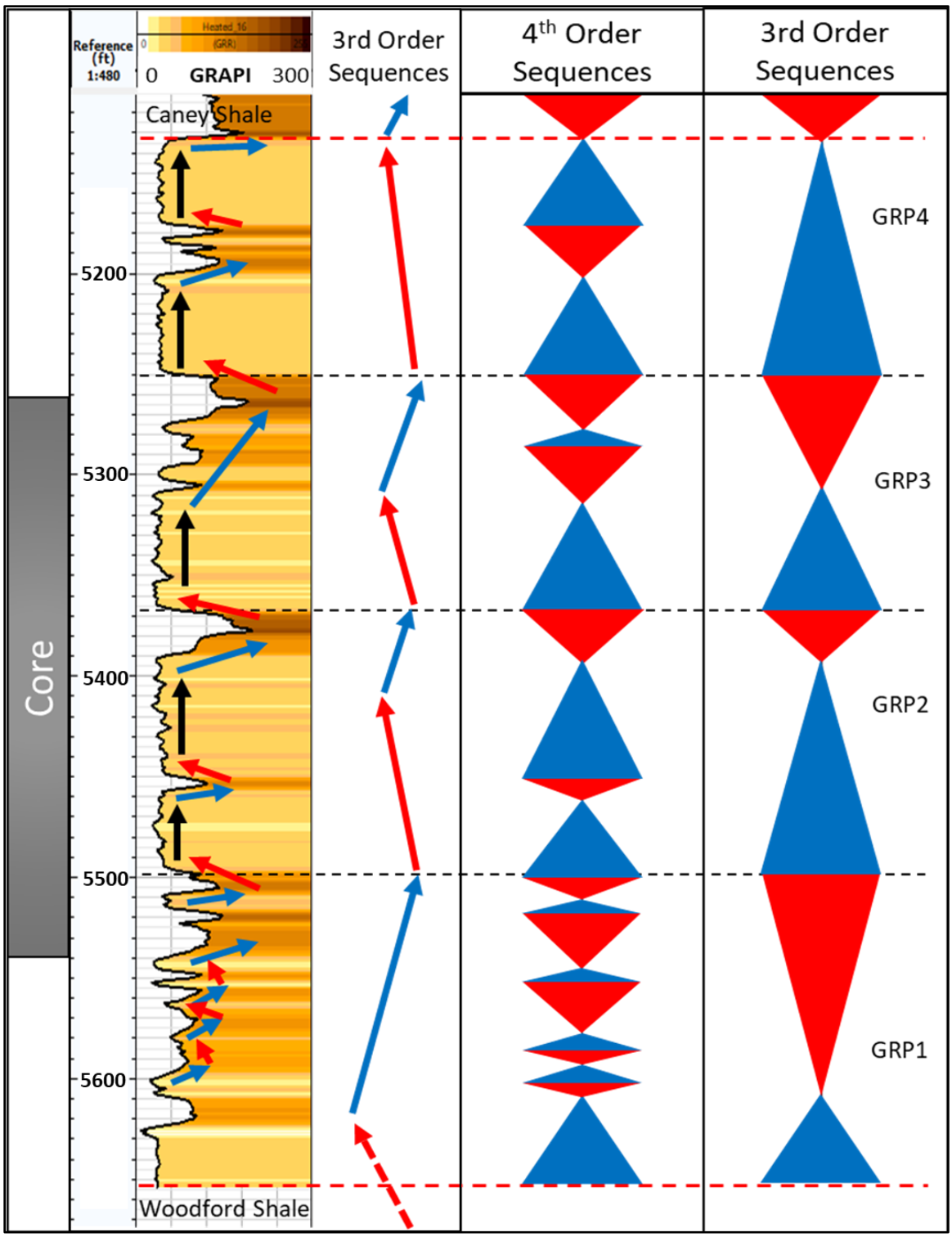

Figure 32: Gamma ray parasequences and hypothesized third and fourth-order sequences. 3rd order parasequences were derrived from major sequence boundaries visible in the chemostratigraphic profiles and those observed in the gamma ray profile. 4th order sequences were derrived using the smaller and shorter lived chemostratigraphic boundaries between Grp1, GRP2, GRP3, and GRP4.

CONCLUSIONS

The Sycamore formation in the Velma field in southern Oklahoma is composed of 10 lithofacies representative of gravity flows, waning sedimentation, and hemipelagic settling or quieter times of deposition. The lithofacies are: (1) laminated mudstones, (2) bioturbated mudstones, (3) laminated bioturbated mudstones, (4) massive siltstones, (5) laminated siltstones, (6) bioturbated siltstones, (7) laminated bioturbated siltstones , (8) massive calcite cemented siltstones, (9) bioturbated calcite cemented siltstones, and (10) interbedded siltstones. Occurrence of these lithofacies is cyclic in nature and suggests compartmentalization internal to the Sycamore formation.

The presence of argillaceous materials and shelf edge ichnofacies, especially in thicker intervals places this section of the Mississippian deposit in a more distal setting. Depositional packages were likely affected by pulses of sedimentation from the Mississippian carbonate system to the north as well as a detrital source that provided the clays and the silt. The fluxes between higher clay supply versus higher silt and carbonate supplies is represented by the variability throughout the rock and in the cyclicity discussed previously, designating the sections internal to the Sycamore.

The system contains some TOC within this region but it is immature. Underlying the Sycamore is the Woodford Shale source rock. The Woodford in this area is viable and charged the shallower Pennsylvanian units, bypassing the Sycamore in the Velma field. The potential of the Sycamore to be charged in deeper settings like the Sholem and Tatums fields remains a question. In this location the Sycamore mudstones with TOC are immature, not contributing to the overall oil generation for the Velma field.

Multivariate cluster analysis shows 7 chemofacies present in the lower to upper Sycamore formation. The precision of the chemofacies is much tighter than that of more traditional methods revealing the degrees to which sections deemed siltstones, in the lithofacies classification, vary chemically. Significant to the idea of calcite dominance within a section is the presence of fractures. Carbonate proxy driven chemofacies reveal denser fracture networks when compared to core observations.

Following the end of the transgressive systems tract that generated the Woodford the Sycamore formation belongs to the distal section of a highstand systems tract that is capped by another transgressive systems tract deposit, the Caney Shale. Internally the Sycamore is compartmentalized by various shale sections and parasequence sets. The units exhibiting greater porosity and permeability are mixed in composition, shale and silt and possess minimal calcite cementation. They do, however, contain dolomite. These units are also the same ones that contain some amounts of TOC (1-2%). If these were subjected to the right temperature, they may be viable source rocks, however the intervals in which they occur are relatively thin (~20 ft. or less) making narrow targets for directional drilling. The upper Sycamore exhibits higher permeability in induction logs and moderate porosity making it a possible reservoir target in an area with petroleum system elements in place.

An alternative interpretation to the characterization of the Sycamore is could be that it was deposited during an overall high stand systems tract phase which had higher orders of cyclicity representing intermediate lowstand and transgressive systems tracts. The well log characteristics for well X-1 resemble those of turbidite deposits in a prograding parasequence set, similar to those described by Slatt, 2013.

RECOMMENDATIONS FOR FUTURE WORK

Moving forward, observance of electrofacies would be useful to relate the chemofacies and lithofacies to electric logs allowing the full upscaling of the analyses. Also incorporating a set of uniaxial confined stress tests would be recommended to understand the rheology of the calcite cemented sections of the Sycamore for fracking purposes.

A spot permeametry study conducted over a breadth of cores from the Ardmore Basin and southern Anadarko Basin areas would be a good future study to begin modeling or mapping the Sycamore. A study to observe specifically calcite cementation and relative locations of higher degrees of cementation would also be useful. These various elements could all also be used in conjunction with mapping to generate a reservoir model for the area further evaluating sections of the Sycamore for potential.

Lastly, an in-depth TOC and Rock Eval analyses are in order for the Sycamore formation's shale intervals. A model for maturity should be generated specifically for the Sycamore mirroring Jarvie's workflow for maturity and hydrocarbon generation potential. This is already discovered for the Barnett and the Woodford. It would be reasonable to consider this for the Sycamore.

REFERENCES

Alpin, A.C., & Macquaker, J.H.S., 2010, Getting started in shales: American Association of Petroleum Geologists/Datapages, Getting Started Series GS20.

Baniak, G. M., Gingras, M., Burns, B., and Pemberton, G., 2015, Petrophysical characterizaiton of bioturbated sandstone reservoir facies in the Upper Jurassic Ula Fomation, Norwegian North Sea, Europe: Journal of Sedimentary Research, v. 85, p. 62-81. DOI:10.2110/jsr.2015.05

Becerra Rondon, D.M., 2017, Integrated Geological Characterization at the bed scale of the Woodford shale at the I-35 outcrop, southern Oklahoma; University of Oklahoma, Thesis.

Becerra, D., Galvis, H., & Slatt, R., 2018, Characterizing the two principal rock types comprising the Woodford Shale resource play: Application to shale geomechanics: SEG & AAPG Interpretation, vol. 6, no.1, p.SC67- SC84.

Bennison, A.P., 1956, Springer and Related Rocks of Oklahoma, Tulsa Geological Society Digest, vol. 24, p. 112.

Blakey, R. C., 2012, Paleogeography of Europe: Colorado Plateau Geosystems: Deep Time Maps, web.

Blatt, H., 1992, Sedimentary Petrology. Freeman, New York, p.514.

Boggs, S., 1995, Principles of Sedimentology and Stratigraphy: Upper Saddle River, New Jersey, Prentice-Hall Inc., p.115.

Brown, D., 2014, Oklahoma Plays Offer Untapped Potential. AAPG Explorer, web access. https://explorer.aapg.org/story/articleid/8045

Brumsack, H. J., 1989, Geochemistry of recent TOC-rich sediments from the Gulf of California and the Black Sea. Geologische Rundschau, v. 78, p. 851-882.

Carpenter, Molly and Tapp, Bryan, 2014, Structural Analysis of Sho-Vel-Tum using balanced cross sections: Oklahoma Geological Survey Guidebook 38, p. 237-340.

Champlin, S.C., 1959, A Stratigraphic Study of the Sycamore and Related Formations in the Eastern Arbuckle Mountains, University of Oklahoma, Masters Thesis.

Coffey, W.S., 2000, The Diagenetic History and Depositional Systeln ofthe Sycamore Formation (Mississippian), Carter-Knox Field, Grady and Stephens Counties, Oklahoma. Oklahoma State University, Dissertation.

Coffey, W.S., 2001, Lithostratigraphy and porosity characterization of the sycamore formation (Mississippian), and it's relationship to reservoir performance, Carter-Knox Field, Grady and Stephens County, Oklahoma. OCGS – Shale Shaker, v.52 (1), p. 9-17.

Cole, T., 1988, A surface to subsurface study of the Sycamore Limestone (Mississippian) along the north flank of the Arbuckle Anticline; University of Oklahoma, Masters Thesis.

Cooper, C.L., 1926, The Sycamore Limestone, Oklahoma Geological Survey, Circular No.9.

Duarte – Coronado, D., 2018, Rock Characterizaiton and Stratigraphy of the Mississisippian Strata, Meramec/Sycamore Merge Play, Central Oklahoma; The University of Oklahoma, Thesis, p.13.

Droser, M.L., & Bottjer, D.J., 1986, A semiquantitative field classification of ichnofabric: Journal of Sedimentary Petrology, v. 56, p. 558–559.

Fay, R.O., 1969, Geology of the Arbuckle Mountains along Interstate 35, Carter and Murray Counties, Oklahoma, Ardmore Geological Society Guidebook, p.1-9, 44-46.

Franklin, K.E., 2002, The Depositional History of the Sycamore Limestone, Oklahoma State University, Thesis.

Guler, C., Thyne, G.D., McCray, J.E., and Turner, A.K., 2002. Evaluation of graphical and multivariate statistical methods for classification of water chemistry data. Hydrogeology Journal, vol.10, p. 455-474.

Johnson, K. S., 2008, Geologic History of Oklahoma: Oklahoma Geological Survey, Educational Publication no. 9, p. 2-8.

Lazar, O.R., Bohacs, K., Macquaker, J. H.S., Schieber, J., & Demko, T.M., 2015, Capturing Key Attributes of Fine-Grained sedimentary rocks in outcrops, cores, and thin secitons: Nomenclature and description guidelines. Journal of Sedimentary Research, vol. 85, p. 230-246, doi: 10.2110/jsr.2015.11.

Leeb, D., 1979, Dynamic hardness testing of metallic materials: NDT International, 12, 274–278, doi: 10.1016/ 0308-9126(79)90087-7.

Milad, B., 2019, Integrated reservoir characterization and geological upscaling for reservoir flow simulations of the Sycamore/Meramec and Hunton Plays in Oklahoma: Doctorate of Philosophy thesis, The University of Oklahoma.

Milad, B., 2019, Outcrop to subsurface reservoir characterization of the Mississippian Play in the SCOOP area, Arbuckle Mountains, Oklahoma, USA; The Univeristy of Oklahoma, Dissertation manuscript.

B. Milad, and R. Slatt, 2019, Outcrop to Subsurface Reservoir Characterization of the Mississippian Sycamore/Meramec Play in the SCOOP Area, Arbuckle Mountains, Oklahoma, USA: Unconventional Resources Technology Conference 991-MS.

Miller, J., 2018. Regional Stratigraphy and Organic Richness of the Mississippian Meramec and Associated Strata, Anadarko Basin, Central Oklahoma. The University of Oklahoma, Thesis.

Miller, J. & Cullen, A., 2018, My Favorite Outcrop: Sycamore Formation I-35 South, Arbuckle Mountains, OK. The Shale Shaker, vol.69, no.82, p. 87-99.

Moore, D. M., and R. C. Reynolds, 1997, X-ray diffraction and the identification and analysis of clay minerals: Oxford University Press.

Morgan, G.D., 1924, Geology of the Stonewall Quadrangle, Oklahoma, Bureau of Geology, Bulletin No.2, p. 48-50.

Perry, W.J., 1988, Tectonic evolution of the Anadarko basin region, Oklahoma: U.S. Geological Survey bulletin; 1866-A.

Potter, P.E. Maynard, J.B., & Pryor, W.A., 1980, Sedimentology of Shale: Study Guide and Reference Source: Berlin, Springer-Verlag, p. 303.

Prestridge, J.D., 1957, A subsurface Stratigraphic Study of the Sycamore Formation in the Ardmore Basin, University of Oklahoma, Masters Thesis.

Ratcliffe, K.T., Wright, A.M., Montgomery, P., Palfrey, A., Vonk, A., Vermeulen, J. and Barrett, M., 2010. Application of chemostratigraphy to the Mungaroo Formation, the Gorgon field, offshore northwest Australia. Australian Petroleum Production and Exploration Association Journal, 50, p.371-385.

Reineck, H.-E., 1963, Sedimentgefüge im Bereich der südlichen Nordsee: Senckenbergische Naturforschende Gesellschaft, Abhandlungen 505, p. 1–138.

Rowe, H., Hughes, N., Robinson, K., 2012a. The quantification and application of handheld energy-dispersive x-ray fluorescence (ED-XRF) in mudrock chemostratigraphy and geochemistry. Chem. Geol. 324–325, 122–131. https://doi.org/10.1016/j.chemgeo.2011.12.023

Ruppel, S.C., Rowe, H., Milliken, K., Gao, C. and Wan, Y., 2017. Facies, rock attributes, stratigraphy, and depositional environments: Yanchang Formation, Central Ordos Basin, China. Interpretation.

Rutledge, R.B., 1956, The Velma Oil Field, Stephens County, Oklahoma in Petroleum Geology of Southern Oklahoma, Ardmore Geological Society, vol. 1, p. 267.

Schieber, J., Krinsley, D., Riciputi, L., 2000, Diagenetic origin of quartz silt in mudstones and implications for silica cycling. Nature 405, p.981-985.

Schieber, J., 2009, Discovery of agglutinated benthic foraminifera in Devonian black shales and their relevance for the redox state of ancient seas: Journal of Paleogeography, Paleoclimatology, Paleoecology, vol. 271, no 3-4, p. 292-300, doi:10.1016/j.paleo.2008.10.027

Schwartzapfel, J.A., 1990, Biostratigraphic Investigations of Late Paleozoic (Upper Devonian to Mississippian) Radiolaria within the Arbuckle Mountains and Ardmore Basin of South-Central Oklahoma, University of Texas at Dallas, Dissertation.

Simpson, M., 2015, A structural re-evaluation of the Ardmore Basin, AAPG Search and Discovery Article #10795.

Slatt, R.M., 2013 Stratigraphic reservoir characterization for petroleum geologists, geophysiscists, and engineers: Origin, recognition, initiation, and reservoir quality, 2nd edition; Developments in Petroleum Science, vol. 61, p. 211-214, 490-495.

Stilwell, H., Martinez, N., Hildred, G. and Zaitlin, B., 2013. Forensic Chemostratigraphy in Geosteering Multilateral Wells: An Example from Devonian to Carboniferous Aged Sequences in Southern Alberta. Unconventional Resources Technology Conference (URTEC).

Taff, J.A., 1903, Geologic Atlas ofthe United States, Tishomingo Folio, Indian Territory, No. 98, p. 5.

Taylor, A.M., & Goldring, R., 1993, Description and analysis of bioturbation and ichnofabrics; Geological Society of London, Journal, v.150, p. 141-148.

Terrell, C., 2019, Regional Stratigraphy and Diagenetic characterization of the Mississippian Meramec, Osage, and Sycamore Formations, Anadarko Basin, Central Oklahoma; University of Oklahoma, Thesis.

Thurston, D. and Taylor, J., 2016, June. Logging for Free-The Use of XRF on Cuttings Data in Unconventional Oil and Gas Exploration and Reservoir Characterization. In SPWLA 57th Annual Logging Symposium. Society of Petrophysicists and Well-Log Analysts.

Turner, B.W., Treanton, J. & Slatt, R., 2016, The use of chemostratigraphy to refine ambiguous sequence stratigraphic correlations in marine mudrocks. An example from the Woodford Shale, Oklahoma, USA. Journal of the Geological Society. doi:10.1144/jgs2015-125

Ward, J.H.,1963, Hierarchical grouping to optimize an objective funciton. Journal of the American Statistical Association, vol. 69, p. 236-244.

Weller, J.M., Williams, J.S., Bell, W.A., Dunbar, C.O., Laudon, L.R., Moore, R.C., Stockdale, P.B., Warren, P.S., Caster, K.E., Cooper, C.L., Willard, B., Croneis, C., Malott, C.A., Price, P.H., & Sutton, A.H., 1948, Correlation of the Mississippian Formations of North America, GSA Bulletin, vol. 59, p. 91–196. doi: https://doi.org/10.1130/0016-7606(1948)59[91:COTMFO]2.0.CO;2

Wright, A.M., K.T. Ratcliffe, and Spain, D.R., 2010. Application of inorganic whole rock geochemistry to shale resource plays. In Canadian Unconventional Resources and International Petroleum Conference. Society of Petroleum Engineers.

APPENDIX

A. Mineralogical Model

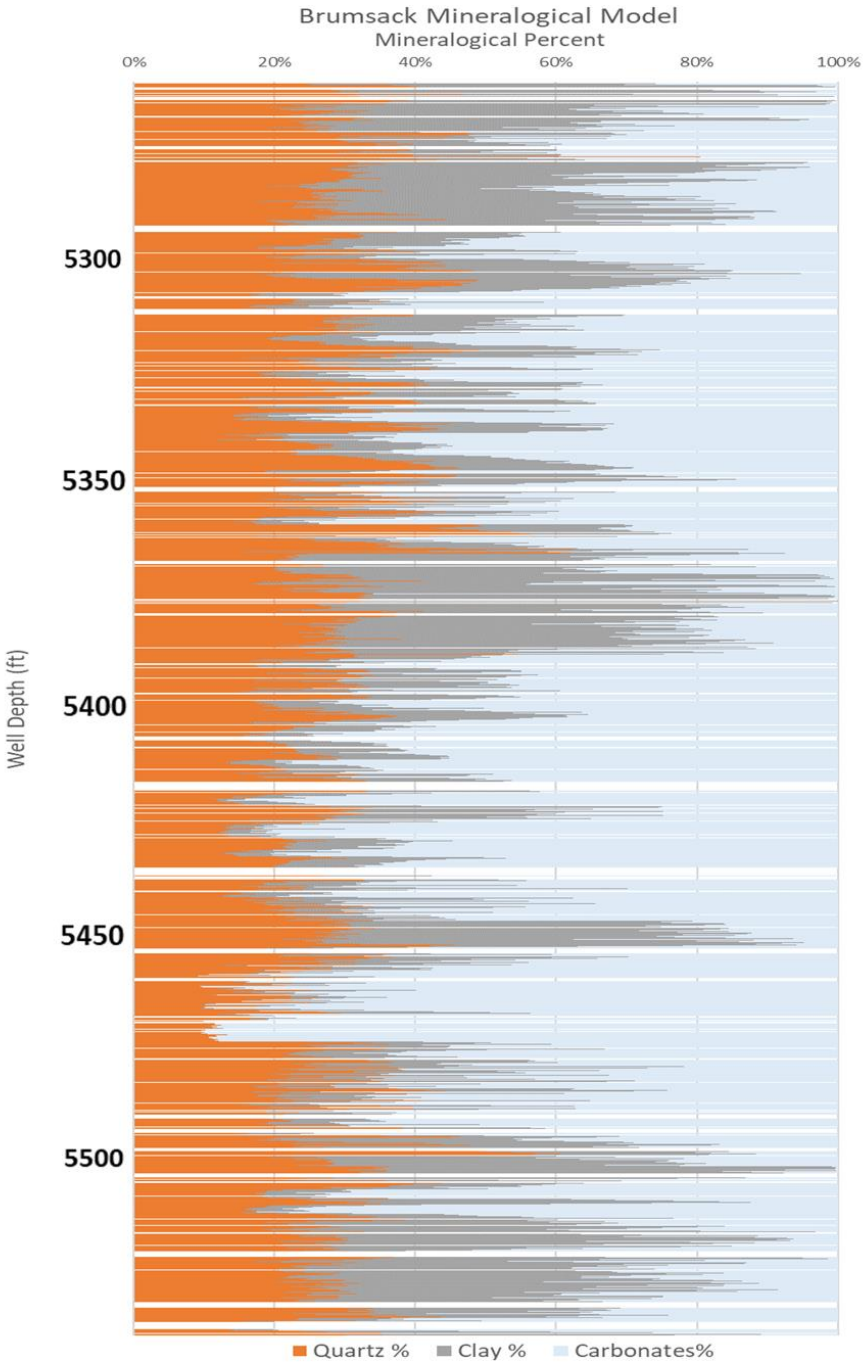

Figure 33: Mineralogical model of the dominant three mineralogies derived from the XRF data. Values here are proxy mineralogies. The values were calculated using the XRF data (in ppm) and equations 5-11 in section 3.1.3.

B. Multivariate Cluster Analyses Results

Class	Ca (ppm)	Mg (ppm)	Al (ppm)	K (ppm)	Si (ppm)	Ti (ppm)	S (ppm)	P (ppm)	Sr (ppm)	Th (ppm)	Si/Al (v/v)	Si/Ti (v/v)	Zr (ppm)	Mo (ppm)	V (ppm)	U (ppm)
1	95,689.40	22,031.94	19,723.84	6,179.45	91,473.65	1,593.01	163,056.15	3,644.36	320.11	8.93	4.76	60.20	203.91	7.79	17.09	11.20
2	45,902.92	3,742.69	38,147.94	14,209.31	231,020.06	3,022.09	41,802.64	897.36	391.93	7.53	8.29	103.28	173.26	11.92	58.30	8.70
3	73,400.28	8,053.91	29,444.82	9,899.13	142,883.89	2,337.34	92,539.13	1,958.88	405.77	8.20	5.16	67.19	189.74	5.81	15.94	10.18
4	125,636.49	2,747.00	14,709.46	4,155.11	188,191.65	1,648.67	14,425.05	1,070.20	633.85	4.13	13.94	134.34	162.42	2.01	56.27	7.31
5	203,425.31	2,166.38	7,663.06	2,463.98	108,674.10	1,454.55	7,994.51	229.65	848.57	3.36	17.96	103.79	111.35	0.49	48.11	6.80
6	178,597.42	3,904.11	12,299.70	3,230.34	158,880.36	1,437.90	8,394.01	521.51	771.49	3.56	13.57	123.54	133.73	0.50	53.36	6.67
7	265,870.29	3,129.60	5,627.63	1,809.11	86,062.75	1,051.54	5,333.73	82.76	944.97	3.05	21.95	95.11	92.57	0.03	52.12	6.53

Table 7: Elemental averages for each cluster.